nature communications

Article

https://doi.org/10.1038/s41467-025-58342-z

p38 mediated ACSL4 phosphorylation drives stress-induced esophageal squamous cell carcinoma growth through Src myristoylation

Received: 30 December 2023

Accepted: 18 March 2025

Published online: 07 April 2025

Check for updates

Qiang Yuan[1,2,3,4], Yunshu Shi[1,2,3,4], Junyong Wang[3], Yifei Xie[1], Xiaoyu Li[1,2,3,4], Jimin Zhao[1,5,6], Yanan Jiang[1,5,6], Yan Qiao[1,5,6], Yaping Guo[1,5,6], Chengjuan Zhang[7], Jing Lu[1,5,6], Tongjin Zhao[1,3,8], Ziming Dong[1,5,6], Peng Li[1,2,3] ✉, Zigang Dong[1,3] ✉ & Kangdong Liu[1,2,3,4,5] ✉

The comprehension of intricate molecular mechanisms underlying how external stimuli promote malignancy is conducive to cancer early prevention. Esophageal squamous cell carcinoma (ESCC) is considered as an external stimuli (hot foods, tobacco, chemo-compounds) induced cancer, characterized by stepwise progression from hyperplasia, dysplasia, carcinoma in situ and invasive carcinoma. However, the underlying molecular mechanism governing the transition from normal epithelium to neoplastic processes in ESCC under persistent external stimuli has remained elusive. Herein, we show that a positive correlation between p38 and ERK1/2 activation during the progression of ESCC. We identify that phosphorylation of ACSL4 at T679 by p38 enhances its enzymatic activity, resulting in increased production of myristoyl-CoA (C14:0 CoA). This subsequently promotes Src myristoylation and activates downstream ERK signaling. Our results partially elucidate the role of ACSL4 in mediating stress-induced signaling pathways that activate growth cascades and contribute to tumorigenesis.

Exposure to harmful external stimuli, such as UV irradiation, hot foods, smoking, chemicals, radiation, and infection, often results in cellular stress responses[1]. Currently, the mechanism of cellular adaptation to stress includes DNA damage response (DDR), the unfolded protein response (UPR), mitochondrial stress signaling, the oxidative stress response and autophagy to support cellular function and maintain cellular, even organismal homeostasis[1–3]. External stimuli, such as UV and ionizing irradiation or pro-inflammatory cytokines, disrupt cellular homeostasis and activate signaling pathways, including p38 MAPK and c-Jun N-terminal kinase (JNK) pathways[4,5]. However, the persistence of external stimuli or repair degeneration over time contributes to the disease development, such as cancer[3]. For instance, defective DDR leads to gene instability and subsequent mutation, which in turn triggers tumor initiation[6,7]. Activation of UPR signaling branches including

[1]The Pathophysiology Department, School of Basic Medical Sciences, Zhengzhou University, Zhengzhou, Henan, China. [2]State Key Laboratory of Metabolic dysregulation & the Prevention and Treatment of Esophageal Cancer, Zhengzhou, Henan, China. [3]Tianjian Laboratory for Advanced Biomedical Sciences, Zhengzhou, Henan, China. [4]China-US (Henan) Hormel Cancer Institute, Zhengzhou, Henan, China. [5]Provincial Cooperative Innovation Center for Cancer Chemoprevention, Zhengzhou University, Zhengzhou, Henan, China. [6]Cancer Chemoprevention International Collaboration Laboratory, Zhengzhou, Henan, China. [7]Center of Bio-Repository, The Affiliated Cancer Hospital of Zhengzhou University, Zhengzhou, China. [8]State Key Laboratory of Genetic Engineering, Shanghai Key Laboratory of Metabolic Remodeling and Health, Institute of Metabolism and Integrative Biology, Zhongshan Hospital, Fudan University, Shanghai Qi Zhi Institute, Shanghai, China. ✉e-mail: li-peng@mail.tsinghua.edu.cn; zgdong@hci-cn.org; kdliu@zzu.edu.cn

IRE1α, PERK, and ATF6 is crucial for restoring ER homeostasis. Interestingly, activation of UPR signaling has also been observed to exhibit hyperactive in multiple tumor types[8,9]. Additionally, numerous studies have demonstrated that the activation of cellular stress-related pathways induces growth signaling. For example, in UV-induced skin carcinogenesis models, the capacity of cell growth increases along with p38 activation[10,11]. Moreover, exposure to chemical agents can induce stem cell properties through JNK signaling, thereby promoting the growth and metastasis of breast cancer[12]. Nevertheless, the precise mechanism by which external stimuli induce stress signaling pathways and activate intracellular proliferation pathways, subsequently promoting tumorigenesis at the molecular level, remains incompletely understood.

Increasing evidence suggests that external stimuli have been recognized as important risk factors in the progression from precancerous lesions to cancer, particularly in digestive tumors[13–15]. The esophagus serves as a conduit connecting the external environment with the internal body, thereby being exposed to extracellular stress factors such as smoking, alcohol consumption, and ingestion of hot foods or beverages[13,16], which are associated with an increased risk of developing ESCC[17–20]. However, the precise mechanisms underlying the impact of external stimuli on proliferation or the crosstalk between stress and growth pathways during the conversion from precancerous lesions to ESCC progression remain incompletely elucidated.

Metabolic reprogramming is recognized as a hallmark of cancer[21]. Aberrant fatty acid (FA) metabolism has been proven in various malignances, where FA can be channeled into various metabolic pathways, including β-oxidation to generate ATP as energy source and serving as a precursor for lipid species to form components of cell membranes by phospholipids, such as glycerophospholipids and sphingolipids, thereby influencing membrane plasticity[22]. Many bioactive lipids are derived from FAs, such as diacylglycerol (DAG) and phosphatidylinositol-3,4,5-trisphosphate (PIP3), act as the second messengers in response to external stimuli[23]. Notably, free fatty acid could be catalyzed into fatty acyl-CoA esters by acyl-CoA synthase, thereby initiating metabolism processes. Among the members of ACSL family, ACSL4 specifically catalyzes free 12–22 carbons long-chain fatty acids[24,25]. *ACSL4* is located at chromosome Xq22.3, which has been firstly reported relation to X-linked the nonspecific mental retardation and fatty acid metabolism[26]. Currently, ACSL4 exhibits elevated expression in ovarian cancer, hepatocellular carcinoma, prostate cancer, colorectal cancer and is associated with an unfavorable prognosis[27,28]. Moreover, some evidence reported that ACSL4 could inhibit cell proliferation via inducing ferroptosis in glioma cells or be involved in chemotherapy resistance by enhancing mitochondrial membrane phospholipid[29–31]. However, the involvement of ACSL4 in stress-inducing growth by reprogramming fatty acid metabolism remains to be elucidated.

Some evidence has indicated that p-p38 and p-ERK simultaneously upregulated in response to stress conditions[11,32]. Our previous research also indicated that sunlight UV strongly leads to an increase of phosphorylation p38 as well as activation of c-jun and CREB, known as transcription factors by ERK[11]. However, the underlying mechanism has not been clearly elucidated.

In this work, we identify a positive association between p-p38 (T180/Y182) and p-ERK1/2 (T202/Y204) in cancer initiation and progression. Importantly, we have identified p38 activates ERK1/2 via phosphorylation of ACSL4 at T679, resulting in producing C14:0 CoA as substrate for Src myristoylation during ESCC development. Our findings elucidate the mechanism by which external stimuli induce stress pathway, activating growth pathway mediated by lipid metabolism in cytoplasm and contributing to tumorigenesis.

Results

Signaling pathways investigation and correlation of p-p38 and p-ERK1/2 under stress stimulus in ESCC tumorigenesis procedure

To investigate the molecular alterations during chronic external stimuli-induced ESCC tumorigenesis, we established the models using normal human esophagus epithelial cells (HET-1A) as well as ESCC cell lines (KYSE150 and KYSE70), subjected to heat stress (42 °C) and chemical carcinogen (4NQO), aiming to simulate the physiological conditions of an esophagus exposed to external stress stimuli. Through screening various stress and cell proliferation signaling molecules, we observed that the levels of p-STAT3 (S727), p-JNK2 (T183/Y185), p-p38 (T180/Y182), p-ERK1/2 (T202/Y204), and p-AKT (S473) were elevated (Fig. 1a, b). Interestingly, treatment with p38 inhibitors (SB202190) resulted in a decrease of p-ERK1/2 (T202/Y204), while no changes were observed upon treatment with JNK or JAK2 inhibitors (Supplementary Fig. 1). These findings suggested a positive correlation between p-p38 (T180/Y182) and p-ERK1/2 (T202/Y204).

To confirm the results observed in vitro, mice were received with 4NQO for varying durations to induce five recognizable precancerous and cancerous lesions in the esophagus (Fig. 1c), which was used to assess the levels of p-p38 (T180/Y182) and p-ERK1/2 (T202/Y204) in the esophagus at different time points in vivo. Results revealed that p-p38 (T180/Y182) and p-ERK1/2 (T202/Y204) were both elevated with the progress of the disease, and activation of p38 and ERK1/2 occurred positive association (Fig. 1d, e), which were consistent with the data in vitro. Meanwhile, we also assessed the association between p-p38 (T180/Y182) and p-ERK1/2 (T202/Y204) in patients' tissues with precancerous lesions and obtained similar results (Fig. 1f and Supplemental Fig. 7). Furthermore, treatment of KYSE150 and KYSE70 cells with structurally unrelated p38 inhibitors (SB202190 and Doramapimod) results in suppression of ERK1/2 phosphorylation at T202/Y204 sites (Fig. 1g and Supplementary Fig. 2a). However, no significant changes were observed in the phosphorylation status of p-p38 (T180/Y182) upon treatment with an ERK inhibitor SCH772984 (Supplementary Fig. 2b). Based on these findings, we hypothesized that p38 could regulate activation of ERK1/2 during ESCC development. However, p38 did not exhibit direct affinity with ERK1/2 or directly phosphorylate ERK1/2 (Supplementary Fig. 2c, d). Hence, we speculate the existence of other molecular entities that mediate the regulatory process.

p38 binds with ACSL4 and phosphorylates ACSL4 at T679 residue

Subsequently, we employed IP/MS analysis to identify a putative mediator that facilitates crosstalk between p38 and ERK signaling pathways during ESCC tumorigenesis. According to the intensity and the number of peptides, we sequentially validate the top 4 candidates (HSPA1A, HSPA8, ACSL4, and HSP90β) (Supplementary Data 1 and Supplementary Fig. 3a, b). The interaction between p38 and HSPA1A (HSP70) induced by environmental stress has been confirmed[33]. Some evidence also confirmed that there is an affinity between p38 and HSP90[34]. ACSL4 medicating fatty acid metabolism is involved in the progression of various cancers. However, whether ACSL4 takes a major role on stress-inducing ESCC development through interacting with p38 has not been investigated. The results presented that ACSL4 could interact with p38 (Fig. 2a). To confirm the result, we performed the CO-IP assays with exogenously expression p38 in HEK293T cells, and Flag-p38 was found to bind with endogenous ACSL4 (Fig. 2b). Computer modeling was conducted to confirm the interaction between p38 and ACSL4. The modeled structure revealed that LYS-360, ILE-110, LEU-102, GLY-358, LYS-357, LYS-117, GLN-109, PRO-110, and GLU-105/107 of ACSL4 bind with ASP-227, SER-252/254, ARG-186, ASP-177, SER61, and THR-175 of p38 (Fig. 2c). Furthermore, Flag-ACSL4 was found to precipitate V5-p38 from HEK293T cell lysates, and vice versa (Fig. 2d). The endogenous interactions between p38 and ACSL4 were also validated in ESCC cell lines (Fig. 2e). Consistently, we performed glutathione S-transferase (GST)

pull-down assay using recombinant ACSL4 protein. GST-ACSL4, but not GST alone, precipitated recombinant Flag-p38 (Supplementary Fig. 3c), indicating a direct interaction between p38 and ACSL4. Moreover, bimolecular fluorescence complementation (BiFC) assay was used to directly visualize p38-ACSL4 interaction ex vivo (Fig. 2f). p38α is known as a serine/threonine protein kinase that phosphorylates its target proteins on Ser-Pro/Thr-Pro sites motif[35]. Therefore, we speculated whether it could phosphorylate ACSL4 at specific sites. Firstly, NetPhos 2.0 server was used to predict the phosphorylation site of ACSL4 by p38. We found p38 could phosphorylate ACSL4 at Thr 679 (T679) (Fig. 2g). Indeed, our results indicated that p38α phosphorylated ACSL4 at T679 from the in vitro kinase assay (Fig. 2h). Remarkably, treatment with p38 inhibitor reduced the levels of ACSL4 phosphorylation (Fig. 2h). Similarly, incubation of the ACSL4-Thr679Ala (T679A) mutant with p38 exhibited impaired phosphorylation (Fig. 2i). These data suggest that p38 phosphorylates ACSL4 at T679. The dimerization of ACSL4 is critical for enzyme activation[36]. Importantly, ACSL4 Thr679Asp (T679D) mutation showed an increased level of ACSL4 dimerization compared to WT group but ACSL4 T679A mutation inhibited dimerization (Fig. 2j). These results indicate that phosphorylation of ACSL4 at T679 by p38 is vital for its enzyme activity and dimerization.

ACSL4 is upregulated in ESCC

To investigate the role of ACSL4 in ESCC, we collected ACSL4 mRNA expression data from GEO datasets (GSE44021 $n = 113$, GSE23400 $n = 53$). The results revealed a significant increase in the expression of ACSL4 in ESCC compared to the paired adjacent tissues (Fig. 3a). Additionally, we also observed a significantly higher level of ACSL4 mRNA in esophageal carcinoma compared to normal tissues from GEPIA database (Fig. 3b). Furthermore, to validate ACSL4 expression further in the context of ESCC, we assessed ACSL4 protein levels by IHC staining in ESCC ($n = 22$) and adjacent tissues ($n = 16$) from patients. The results revealed a higher level of ACSL4 in ESCC tissues than paired adjacent tissues (Fig. 3c, d and Supplemental Fig. 8). Consistent with these results, IHC staining of ESCC tissue microarray revealed that ACSL4 protein levels were significantly increased in ESCC compared with the corresponding adjacent tissues (Fig. 3e, f and Supplemental Fig. 9). In addition, clinical correlation analysis uncovered that ACSL4 level was notably related with age and pathological grade of ESCC (Table 1). Furthermore, the results of Kaplan–Meier analysis suggested that the ESCC patients with low ACSL4 protein levels had better overall survival than those with high ACSL4 protein levels (Log-rank $P = 0.0455$, Fig. 3g). Moreover, ESCC tissues showed

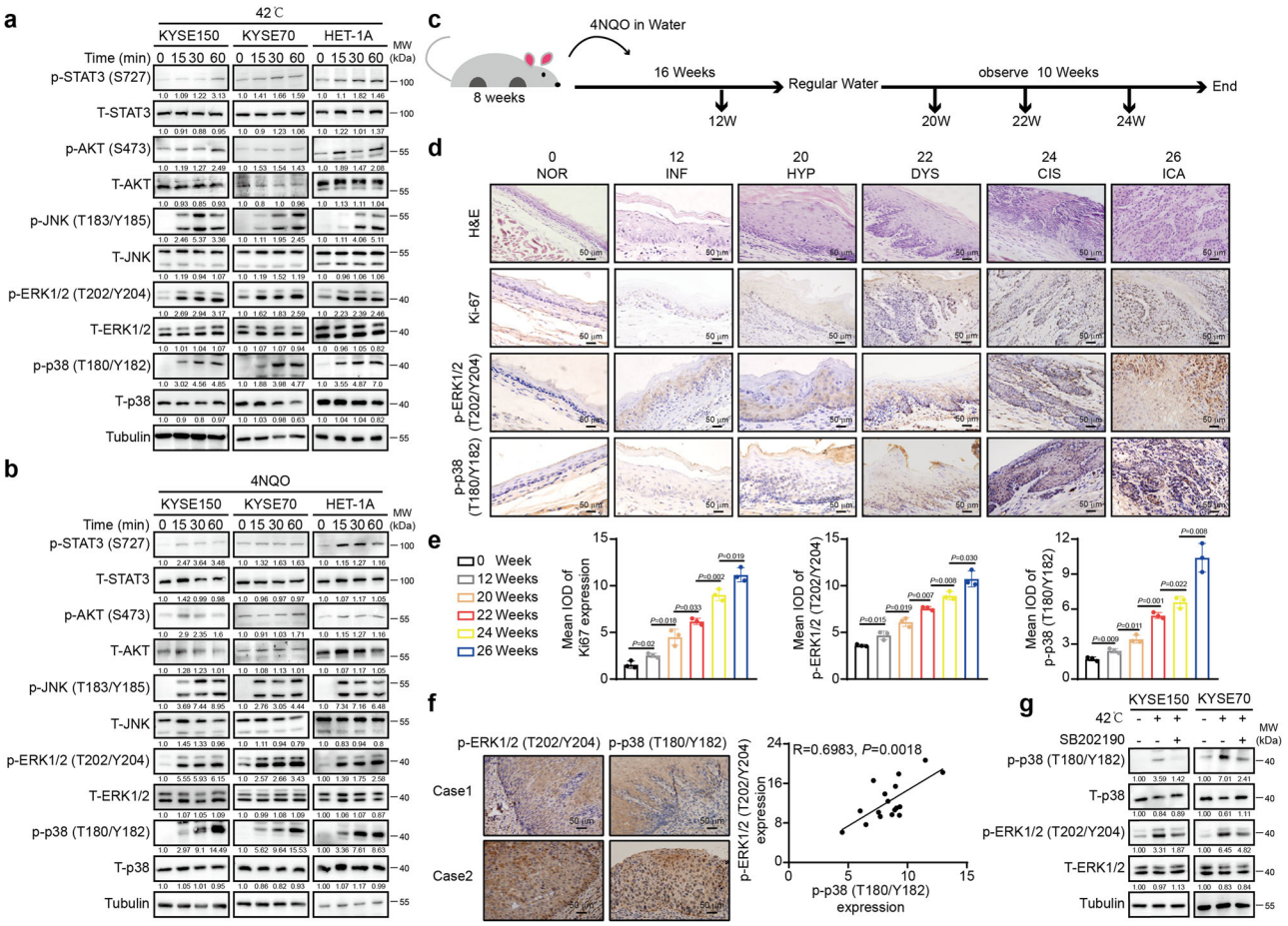

Fig. 1 | Signaling pathways investigation and p-p38 and p-ERK1/2 correlation under stress stimulus in ESCC tumorigenesis procedure. a Screening stress and proliferation related signaling molecules using heat stress. **b** Screening stress and proliferation related signaling molecules using 4NQO. **c** Establishing a mouse model of esophageal precancerous lesions and ESCC induced by 4NQO. Mice were given with 4NQO (100 μg/mL) in drinking water for 16 weeks and then kept regular drinking water for another 10 weeks. Mice were offered euthanasia at week 0, 12, 20, 22, 24, or 26 weeks, respectively. Created by Adobe Illustrator. **d** The samples were harvested and stained with H&E staining and IHC analysis of Ki67, p-ERK1/2 (T202/Y204), and p-p38 (T180/Y182). **e** Protein levels of Ki67, p-ERK1/2 (T202/Y204), and p-p38 (T180/Y182) at different time points. Statistical significance was conducted by two-sided unpaired Student's *t*-test, $n = 3$ samples detected from 3 independent mice. Error bars show the mean ± SD. **f** Representative p-p38 (T180/Y182) and p-ERK1/2 (T202/Y204) IHC staining on human precancerous lesions tissue. $n = 17$, and statistical analysis was conducted by Spearman correlation test. **g** After treatment with 20 μM SB202190 for 2 h followed by heat stress for 1 h, KYSE 70 and KYSE150 cells were subjected to Western blot analysis. Representative immunoblots shown in figures were repeated three times independently with similar results. Source data are provided as a Source Data file.

https://doi.org/10.1038/s41467-025-58342-z

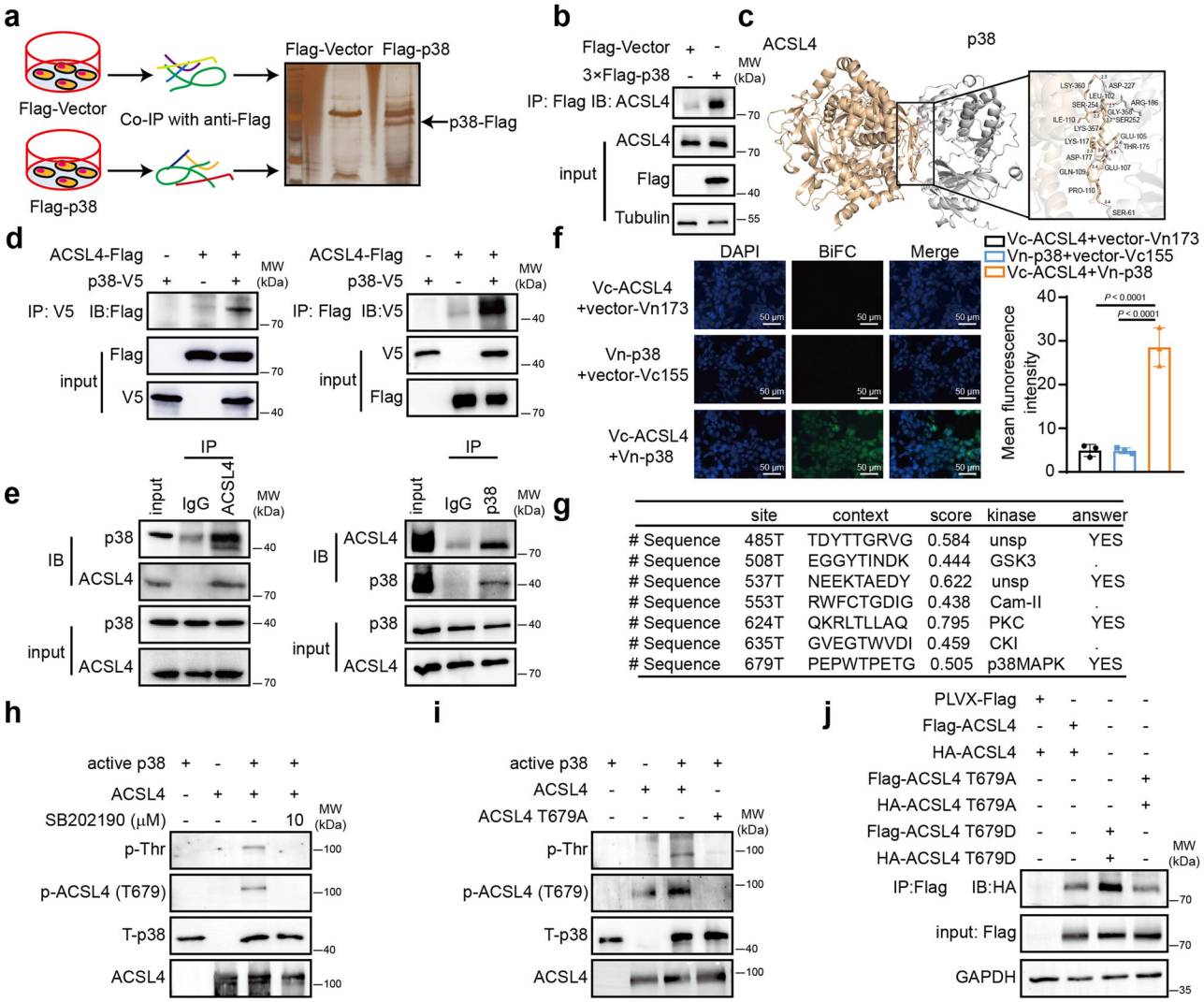

	site	context	score	kinase	answer
# Sequence	485T	TDYTTGRVG	0.584	unsp	YES
# Sequence	508T	EGGYTINDK	0.444	GSK3	.
# Sequence	537T	NEEKTAEDY	0.622	unsp	YES
# Sequence	553T	RWFCTGDIG	0.438	Cam-II	.
# Sequence	624T	QKRLTLLAQ	0.795	PKC	YES
# Sequence	635T	GVEGTWVDI	0.459	CKI	.
# Sequence	679T	PEPWTPETG	0.505	p38MAPK	YES

Fig. 2 | p38 binds and phosphorylates ACSL4 in vitro. a The proteins that bind with p38 were identified by IP/MS analysis. Created by Adobe Illustrator. **b** p38 binds to ACSL4. Beads coated with p38-3 × Flag fusion were incubated with cell lysate. Endogenous ACSL4 was detected by Western blot. **c** Modeling of p38 binding with ACSL4. ACSL4 is colored brown, and p38 is colored gray. **d** p38 and ACSL4 bind with each other exogenously. Flag-ACSL4, V5-p38 plasmids were co-transfected into HEK293T cells. Proteins were extracted after 36 h transfection. The V5- or Flag-tagged proteins were immunoprecipitated with anti-V5 (left) or anti-Flag (right), and then Western blot was performed. **e** p38 and ACSL4 bind with each other endogenously. Proteins extracted from KYSE150 were immunoprecipitated by anti-ACSL4 (left) or anti-p38 (right), and immunoprecipitated complexes were detected using the indicated antibody. **f** BiFC Assay was used to visualize p38-ACSL4 interaction in vivo. Vc-ACSL4, Vn-p38 and vector plasmids were co-transfected into HEK293T cells. After 36 h transfection, green fluorescence was observed. Results are shown as mean ± SD, $n = 3$ biological replicates. P values were determined using one-way ANOVA. **g** The phosphorylated site of ACSL4 by p38 was predicted using NetPhos 2.0 web server. **h** p38 kinase phosphorylates ACSL4 at T679 in vitro. Active p38 protein was incubated with ACSL4-GST fusion protein or simultaneously treatment with 10 μM SB202190. **i** Active p38 protein was incubated with ACSL4-3 × Flag fusion protein or harboring ACSL4-T679A-3 × Flag mutation protein in kinase reaction buffer and then checked by Western blot using antibodies as indicated. **j** Phosphorylation of ACSL4 at Thr679 was essential for its enzyme activity and dimerization. HEK293T cells were co-transfected with Flag-ACSL4 and HA-ACSL4 plasmids or with Flag-ACSL4-T679A and HA-ACSL4-T679A, Flag-ACSL4-T679D and HA-ACSL4-T679D plasmids. The protein was prepared, and Flag-ACSL4 was immunoprecipitated, followed by Western blot analysis using an anti-HA antibody. Representative immunoblots shown in figures were repeated three times independently with similar results. Source data are provided as a Source Data file.

notably increased ACSL4 protein levels compared to normal and adjacent tissues by Western blot (Fig. 3h). Collectively, our data suggest that ACSL4 is upregulated in patients with ESCC, and a high level of ACSL4 is related with poor prognosis.

Elevated ACSL4 and phosphorylation of ACSL4 at T679 are associated with ESCC tumorigenesis and progression in vitro and in vivo

To explore the role of ACSL4 in ESCC cells, we established stable ACSL4 knockdown cell lines (Fig. 4a). MTT, colon formation and soft agar assays were performed. The results demonstrated that the cell proliferation and colony formation ability and anchorage-independent growth were weakened in cells with stable expression of ACSL4 shRNA (Fig. 4b–f). To further elucidate the tumorigenic capacity of ACSL4 in ESCC cells, we performed CDX model in mice subcutaneously injected with ACSL4 silencing cells. The findings demonstrated a significant inhibition of xenograft growth upon ACSL4 knockdown (Fig. 4g). Meanwhile, we noticed that tumor volume in shACSL4 inoculated mice was significantly decreased compared to shMock group mice (taking KYSE70 cells for example: average volume is 795.05 mm^3 in KYSE70 shMock group, 307.76 mm^3 in KYSE70 sh-1group and 240.11 mm^3 in KYSE70 sh-5 group) (Fig. 4h). ACSL4 knockdown groups exhibited a significant decrease in average tumor weights, and sh-1 group decreased by 65.83% and sh-5 group decrease by 50.23% for

https://doi.org/10.1038/s41467-025-58342-z

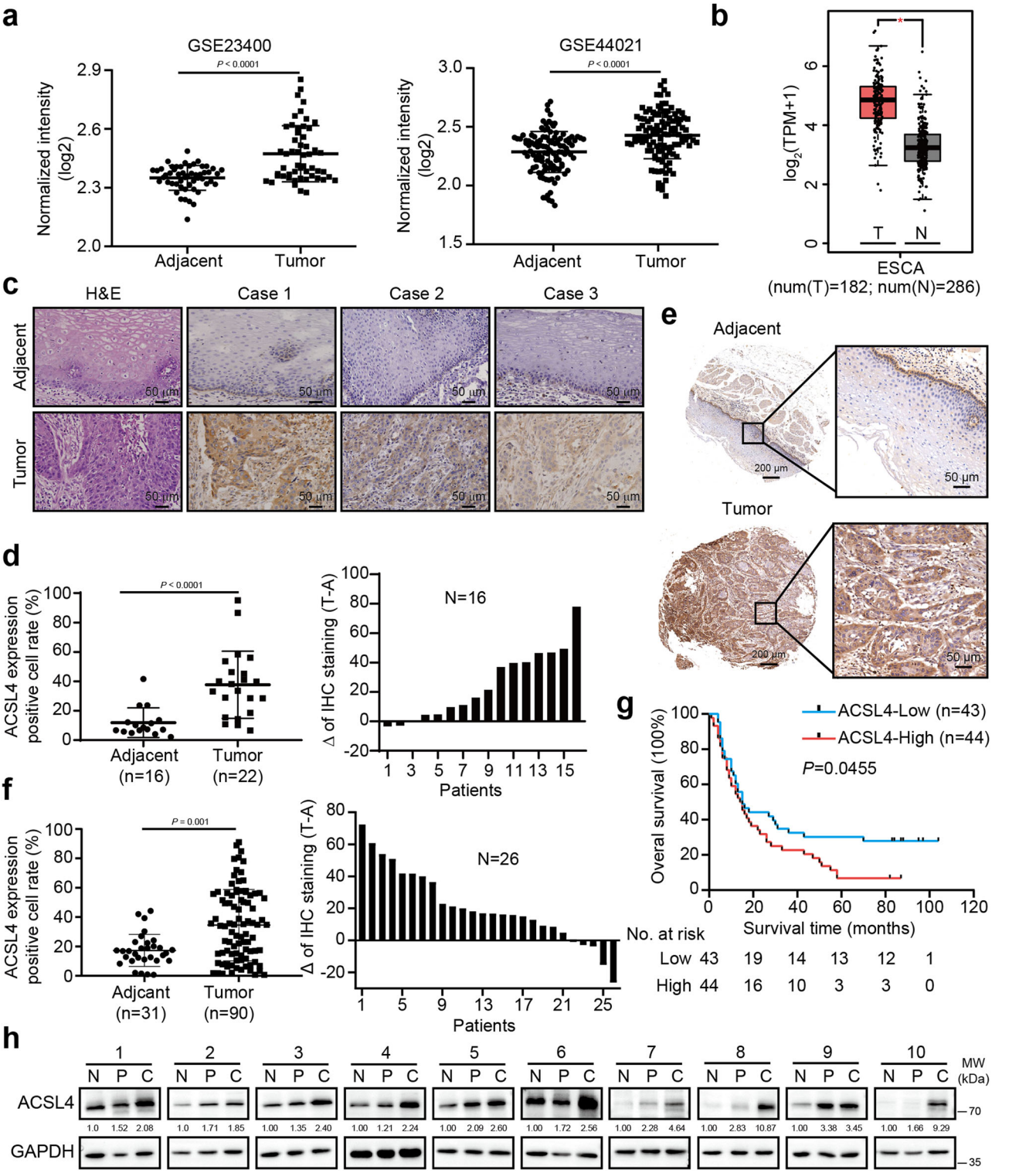

Fig. 3 | ACSL4 is upregulated in ESCC and is related with patient survival probability. a Plots showing ACSL4 transcript expression levels in two paired adjacent-tumor ESCC datasets from GEO. GSE23400, $n = 53$ per group; GSE44021, $n = 113$ per group. For the comparison of ACSL4 expression between adjacent and tumor group: GSE23400 by Mann–Whitney *U* test; GSE44021 by two-sided unpaired Student's *t*-test. **b** mRNA levels analysis of ACSL4 in normal and esophageal carcinoma tissues retrieved from the GEPIA database. TPM Transcripts Per Million. Characteristics of the boxplot in (**b**) (median of $\log_2$TPM + 1): ACSL4 in normal tissue (3.24), tumor tissue (4.86). **c** IHC staining of human ESCC tissues elucidated by ACSL4 antibody. Tissue specimens are from the Henan Cancer Hospital including 16 adjacent tissues and 22 tumor tissues. **d** Analysis of ACSL4 protein levels. **e** IHC staining images of human ESCC tissue microarray using ACSL4 antibody. **f** ACSL4 protein levels were analyzed in paired adjacent and ESCC tissues. Data of (**d** and **f**) are shown as mean ± SD, and *P* value was determined by Mann–Whitney *U* test. **g** Relationship between ACSL4 protein levels and overall survival of patients in ESCC tissue microarray. *P* value was determined by Kaplan–Meier analysis. **h** Protein levels of ACSL4 in 10 paired human clinical samples with ESCC and adjacent tissues. Normal esophageal epithelium (N), paracancer tissue (P) and cancer tissue (C) were examined. Representative immunoblots shown in figures were repeated three times independently with similar results. Source data are provided as a Source Data file.

Table 1 | Correlation between ACSL4 expression and clinicopathological characteristics of ESCC

Characteristics	ESCC (*n* = 90)	Percent	ACSL4		*P* value
			Low (*n* = 45)	High (*n* = 45)	
Gender					0.141
Male	68	75.56%	31 (68.89%)	37 (82.22%)	
Female	22	24.44%	14 (31.11%)	8 (17.78%)	
Age (29–84)					0.026
>65.81	46	51.11%	28 (62.22%)	18 (40%)	
<65.81	43	47.78%	16 (35.56%)	27 (60%)	
Missing	1	1.11%	1 (2.22%)		
Pathological grade					0.034
I	8	8.89%	7 (15.56%)	1 (2.22%)	
II	66	73.33%	33 (73.33%)	33 (73.33%)	
III	16	17.78%	5 (11.11%)	11 (24.44%)	
Tumor volume (mm^3)	Mean value	25.91	24.11	27.88	
Lymph node	Mean value	1.82	1.29	2.37	
pT status					0.590
T1	3	3.33%	1 (2.22%)	2 (4.44%)	
T2	15	16.67%	6 (13.33%)	9 (20%)	
T3	67	74.44%	35 (77.78%)	32 (71.11%)	
T4	1	1.11%	0 (0%)	1 (2.22%)	
Missing	4	4.44%	3 (6.67%)	1 (2.22%)	
Pathomorphology					0.237
Medullary type	23	25.56%	14 (31.11%)	9 (20%)	
Ulcerative type	46	51.11%	21 (46.47%)	25 (55.56%)	
Mushroom umbrella type	5	5.56%	4 (8.89%)	1 (2.22%)	
others	16	17.78%	6 (13.33%)	10 (22.22%)	

KYSE70 cells (Fig. 4i). Moreover, IHC analysis showed a significant decrease in the percentage of Ki67-positive cells within tumors formed by ACSL4 knockdown cells compared to controls (Supplementary Fig. 3d, e). These results suggest that ACSL4 contributes to ESCC progression. To further confirm the oncogenic function of ACSL4, we overexpressed ACSL4 in KYSE450 cells. Our findings demonstrated that ACSL4 expression promoted cell proliferation and colony formation (Supplementary Fig. 3f, g).

Subsequently, we explored the biological function of ACSL4 T679 in ESCC. Our results indicated that phosphorylation of ACSL4 at T679 was higher in tumor than adjacent tissue (Supplementary Fig. 3h). In addition, we stably transfected vector as control, ACSL4-WT, ACSL4-T679A or ACSL4-T679D in KYSE450 cells to determine the biological functions of ACSL4 Thr679 phosphorylation. The cell proliferation and colony formation were significantly reduced in ACSL4-T679A cells compared to ACSL4-WT cells, whereas the ACSL4-T679D mutant exhibited a proliferation-promoting effect (Fig. 4j, k). Additional rescue analysis revealed similar results in ACSL4 knockout cells (Fig. 4l, m). Next, the stably transfected cells with ACSL4-WT, ACSL4-T679A or ACSL4-T679D and vector as control group were delivered subcutaneously to mice. Mice treated with ACSL4-T679D exhibited larger tumors and exhibited higher Ki67 percentage, but ACSL4-T679A mutation group had the opposite effect (Fig. 4n–p and Supplementary Fig. 3i). The results demonstrated that Thr679 phosphorylation mediated by p38 was critical for the activation and improved proliferative capabilities of ACSL4.

Phosphorylation of ACSL4 by p38 activates ERK pathway through Src myristoylation

ACSL4 catalyzes a diverse range of fatty acid substrates, converting them into their corresponding acyl-CoAs, which are essential for various physiological processes including lipid modifications. Notably, lipid attachment was recognized as one of the most common posttranslational modifications in mammalian[37]. A previous study indicates that ACSL4 is involved in protein myristoylation[28]. Therefore, we hypothesized whether ACSL4 modulated myristoylation in the development of ESCC. To support the hypothesis, we measured the levels of C14:0 CoA, which served as the substrate for myristoylation using LC/MS. We achieved good separation by LC/MS methods (Supplementary Fig. 3j). The results indicated knockdown of ACSL4 significantly suppressed synthesis of C14:0 CoA (sh-1 decrease by 27% in KYSE150 cells and 16% in KYSE70 cells; sh-5 decrease by 63% in KYSE150 cells and 32% in KYSE70 cells) (Fig. 5a). Myristoylation is essential for Src kinase activity and function[38]. Therefore, the myristoylation of Src was detected using click chemistry. Our results suggested that knockdown of ACSL4 reduced the levels of myristoylated Src compared to the control group (Fig. 5b). Given that phosphorylation T679 by p38α increased ACSL4 activity, we further investigated its role in Src myristoylation. Indeed, cells transfected with ACSL4-WT exhibited enhanced production of C14:0 CoA (Fig. 5c) and higher level Src myristoylation than vector group (Fig. 5d). Moreover, ACSL4-T679D overexpressed cells demonstrated even higher levels than WT cells, while the ACSL4-T679A overexpressed group displayed an obvious reduction in C14:0 CoA production by approximately 13% compared to WT cells, and a decrease of Src myristoylation (Fig. 5c). To further confirm the role of ACSL4 in Src myristoylation in ESCC, we also excluded the effects of other members of the family (ACSL1, ACSL3, ACSL5, and ACSL6). The results showed that ACSL4 increased in cancer tissue in GEPIA database (Supplement Fig. 4a and Fig. 3b). Moreover, we found that ACSL4 has a significantly expression advantage in another 10 cases of ESCC compared with other members (Supplement Fig. 4b, c). Additionally, we found that knockdown of ACSL4 could significantly

https://doi.org/10.1038/s41467-025-58342-z

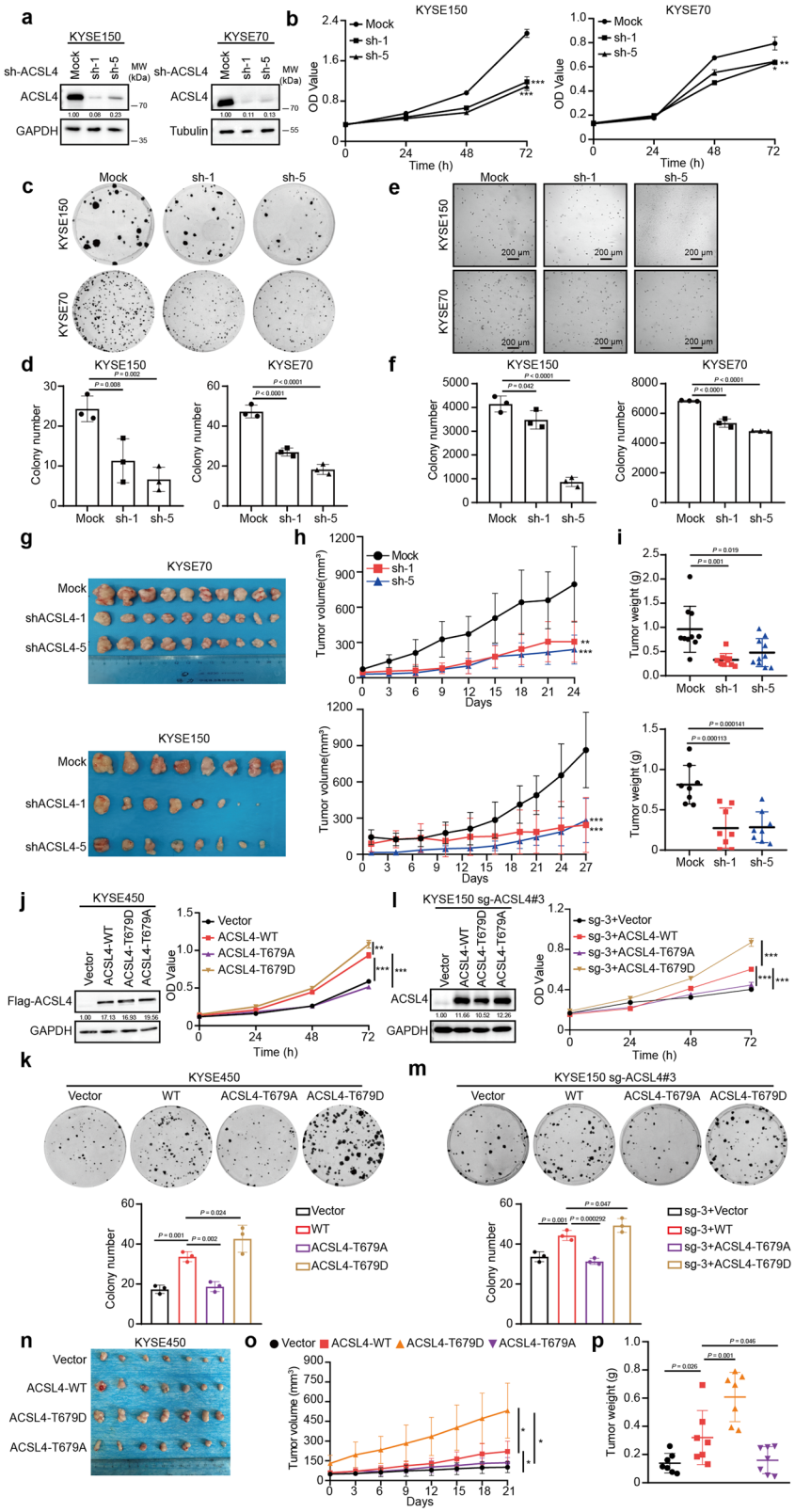

inhibit the Src myristoylation, while the effects of other members present a weak efficacy (Supplement Fig. 4d).

Once activated, Src acts as an upstream regulator of the MAPK/ERK pathway in driving the cancer malignant phenotype of cancer[39]. Subsequently, we check the phosphorylation levels of MAPK/ERK pathway. The results demonstrated that ACSL4 low expression was associated with decreased lower p-Src S416, p-CRAF S338, p-MEK (S217/221), and p-ERK1/2 (T202/Y204) levels (Fig. 5e left). Consistent with the activity of ACSL4, Western blot analysis revealed that the levels of p-Src S416 and MAPK/ERK signals decreased in ACSL4-T679A transfected cells compared to ACSL4-WT cells, while ACSL4-T679D effectively enhanced activation of these signaling pathways (Fig. 5e right).

Consequently, we aimed to validate phosphorylation T679 of ACSL4 by p38 was involved in the regulation of ERK1/2 activation. To

Fig. 4 | ACSL4 and phosphorylation of ACSL4 at T679 promote ESCC tumorigenesis and progression. a KYSE150 and KYSE70 cells with ACSL4 knockdown were established and Western blot was performed to determine the protein levels of ACSL4. **b** Cell growth was measured by MTT assay ($n = 5$ independent experiments). Data were presented as means ± SD. *** $P < 0.0001$ for KYSE150 at 72 h by One-way ANOVA; ** $P = 0.005$, * $P = 0.01$ for KYSE70 at 72 h by One-way ANOVA. **c**, **d** Plate colony formation assay and soft agar assay (**e**, **f**) were measured ($n = 3$ independent experiments). *P* value was determined by One-way ANOVA. **g** KYSE150 and KYSE70 cells with ACSL4 knockdown were subcutaneously injected in mice back to establish CDX models. When the average tumor volume reached 100 mm^3 in mock group, the tumor volume was recorded. (KYSE70: $n = 10$ per group; KYSE150: $n = 8$ per group). **h** Tumor volumes were recorded at two times per week. For KYSE70, **$P = 0.001$, ***$P = 0.000381$ by Mann–Whitney *U* test; KYSE150, mock vs sh-1, *** $P < 0.0001$, mock vs sh-5, ***$P = 0.000116$ by One-way ANOVA. **i** Tumor weights were measured after tumor tissues deprived from mice. For KYSE70, *P* values were determined by Mann–Whitney *U* test; For KYSE150, *P* values were determined by One-way ANOVA. **j** The proliferation ability in cells transfected with T679A or T679D mutation of ACSL4 was determined by MTT assay (right). $n = 6$ biological replicates. For the proliferation comparison of vector and ACSL4-WT, *** $P < 0.0001$; ACSL4-WT vs ACSL4-T679A, *** $P < 0.0001$ by One-way ANOVA; ACSL4-WT vs ACSL4-T679D, ** $P = 0.004$ by Mann–Whitney *U* test. (left) Western blot was performed to determine transfection efficiency. **k** Colony formation in KYSE450 cells transfected with different ACSL4 T679 mutations. $n = 3$ biological replicates. *P* values were determined by One-way ANOVA. **l** The proliferation ability in ACSL4 knock out cells transfected with T679A or T679D mutation of ACSL4 was determined by MTT assay (right) ($n = 5$ biological replicates). *P* values were determined by One-way ANOVA. *** $P < 0.0001$. (left) Western blot was performed to determine transfection efficiency. **m** Colony formation in ACSL4 knock out cells transfected with different ACSL4 T679 mutations. $n = 3$ biological replicates. *P* values were determined by One-way ANOVA. **n** KYSE 450 cells with ACSL4-WT, ACSL4-T679A, ACSL4-T679D or vector were subcutaneously injected in mice back to establish CDX model. When the average tumor volume reached 100 mm^3 in ACSL4-T679D group, the tumor volume was recorded. **o** Tumor volume was monitored twice per week ($n = 7$ per group). *P* values were determined by One-way ANOVA. For tumor volume comparison of vector and ACSL4-WT, * $P = 0.035$; ACSL4-WT vs ACSL4-T679D, * $P = 0.040$; ACSL4-T679D vs ACSL4-T679A, * $P = 0.013$. **p** The weight of the tumors was measured. Data were presented as means ± SD. *P* values were determined by One-way ANOVA. Representative immunoblots shown in figures were repeated three times independently with similar results. Source data are provided as a Source Data file.

model the environmental factors contributing to ESCC initiation and progression, 4NQO treatment and heat stress were employed. The results presented that p-p38 (T180/Y182) and p-ERK1/2 (T202/Y204) increased due to exposure to external stimulus. The activation of p38, acting as an upstream regulator, preceded the activation of ERK under both starved and non-starved conditions (Supplementary Fig. 5a, b). Similarly, as the duration of external stimulus extends, we observed that p-p38 (T180/Y182) and p-ERK1/2 (T202/Y204) elevated gradually, and p-ACSL4 (T679) also increased after 4NQO and heat stress treatment with the activation of p38 and ERK1/2 (Fig. 5f). Furthermore, consistent with the former mentioned trends of p-p38 (T180/Y182), and p-ERK1/2 (T202/Y204), a progressive rise in p-ACSL4 (T679) was observed during 4NQO-induced mouse ESCC tumorigenesis (Fig. 5g). Moreover, the pre-treatment with p38 inhibitor resulted in a simultaneous reversal of p-p38 (T180/Y182), p-ERK1/2 (T202/Y204), and p-ACSL4 (T679) after inducing cellular stress at 42 °C (Fig. 5h). Conversely, we employed the p38 activator LPS to infer the effects and induce alterations. These findings demonstrated that in KYSE150 and KYSE70 cells with ACSL4 knockdown, LPS treatment resulted in a diminished phosphorylation of ERK1/2 compared to sh-mock group (Fig. 5i). However, rescue with ACSL4-T679D in ACSL4 silencing cells resulted in increasing p-ERK1/2 (T202/Y204) levels than sh-group followed by 42 °C to induce p38 activation. In contrast, ACSL4-T679A cells exhibited no change in p-ERK1/2 (T202/Y204) levels (Fig. 5j). Some evidence reveals that the proliferation of triple negative breast cancer cells required Src-dependent p38 activity[40]. Others have demonstrated that p38 also alters Src to activate Erα signaling[41]. After treatment with Src inhibitor (Saracatinib), the results showed that p-ERK1/2 (T202/Y204) decreased upon the drug, but p-p38 also underwent a trend of reducing (Supplement Fig. 5c). In the study, we emphasize that p38 promotes activation of the ERK-related proliferative pathway through phosphorylation of ACSL4 involved in Src myristoylation modification, which is essential for Src activity. However, we do not exclude the fact that there is also a regulatory effect of activated Src on p38 and ERK1/2. Therefore, we enriched the regulatory mechanism between p38, Src and ERK1/2 and there is a crosstalk among them.

Together, these results demonstrate that p38 activates p-ERK1/2 (T202/Y204) via Src myristoylation by phosphorylation ACSL4 at T679.

Acsl4 knockout suppressed tumorigenesis in 4NQO-induced mice model depending on p38/ACSL4/ERK axis

The above results promote us to reveal the functional significance of ACSL4 in ESCC tumorigenesis using 4NQO-induced tumor model. We crossed *Acsl4*$^{fl/fl}$ mice with ED-L2-Cre mice to generate *Acsl4* conditional knockout (CKO) mice in esophagus[42,43]. 4NQO was utilized to promote the ESCC development. Genotyping of *Acsl4* wild-type (WT) and CKO mice was identified via PCR (Fig. 6a), and IHC was performed to estimate ACSL4 expression in mice with different genotypes (Fig. 6b). The body weight of mice significantly decreased after treatment with 4NQO, but mice with *Acsl4* CKO exhibited no significant difference in body weight compared to the WT group due to the agent's toxic side effects (Supplementary Fig. 3k). Furthermore, the overall survival time of 4NQO-induced WT mice was shorter than that of CKO mice based on Kaplan–Meier survival curves (Log-rank $P = 0.0424$) (Fig. 6c). Notably, upon treatment with 4NQO, the surfaces of the esophagus appeared roughened but this effect seemed to be alleviated in CKO mice (Fig. 6d). The results proved that *Acsl4* deletion led to a significant reduction of approximately 25% in the occurrence of 4NQO induced-esophageal tumorigenesis (Fig. 6e). Additionally, the esophagus in CKO group showed a significantly greater length compared to WT group (Fig. 6f). Meanwhile, the CKO group exhibited a significantly smaller average tumor volume compared to WT mice (68% decrease in CKO), while WT mice showed an increased esophagus weight following 4NQO treatment (a 25% decrease in CKO) (Fig. 6g, h). Moreover, most esophagus neoplasms were histologically recognized as squamous cell carcinoma in 4NQO-treated mice by HE staining, while control groups without 4NQO treatment had no tumor (Fig. 6i). Despite *Acsl4* being located on the X-chromosome, we did not observe a surplus of tumor formation in females over males due to no a marked divergence of ACSL4 protein expression between genders (Supplementary Fig. 6). Ki67 protein levels were also significantly decreased in CKO mice compared with WT group. Consistent with previous results, CKO group exhibited lower p-ERK1/2 (T202/Y204), p-Src (S416) compared to WT mice, but no significant changes in p-p38 (T180/Y182) (Fig. 6j). The data suggested that ACSL4 had a promotive impact on ESCC tumorigenesis and enhanced the progression of tumor induced by 4NQO through Src/ERK pathway via p38 activation.

Discussion

Numerous studies have shown that environmental insults inducing stress pathways lead to tumor proliferation through activating growth pathway in ESCC, ovarian cancer, colorectal cancer and other malignancies[44–46]. In response to external stimuli, cellular stress responses act as repair systems for environment variations[47]. However, defects in repair mechanisms play diverse roles in promoting tumor development[6]. The components of these responses, such as XBP1, CHOP, and GRP94 for UPR, have been activated in many tumor

https://doi.org/10.1038/s41467-025-58342-z

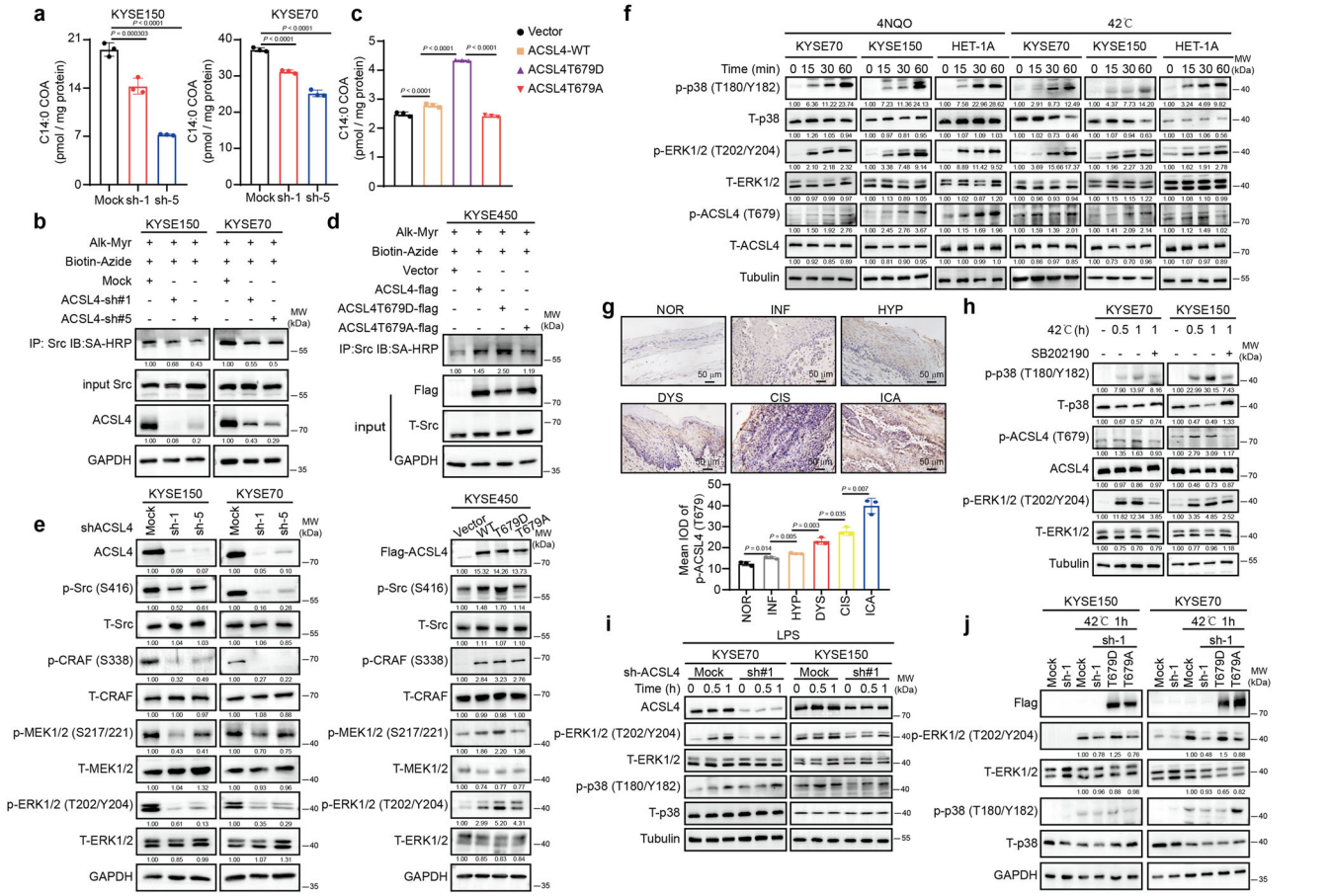

Fig. 5 | Phosphorylation of ACSL4 at T679 site is critical for ACSL4 oncogenic function through Src myristoylation via Src/ERK pathway. a The production of C14:0 CoA in KYSE150 and KYSE70 cells transfected with ACSL4 knock down or sh-Mock as control group ($n = 3$ biological replicates, mean ± SD). *P* values were determined by One-way ANOVA. **b** KYSE150 and KYSE70 cells transfected with shRNA-Mock, shRNA-ACSL4#1, or shRNA-ACSL4#5 by lentiviral infection were cultured with 50 μM myristic acid-alkynyl (Alk-myr) overnight. The protein was extracted, and Src was enriched using anti-Src antibody. Then Src myristoylation in samples was analyzed by Click Chemistry, and detected by streptavidin-HRP (SA-HRP) (**c**) The production of C14:0 CoA in KYSE450 cells transfected with vector, ACSL4-flag, ACSL4-T679A-flag, and ACSL4-T679D-flag ($n = 3$ biological replicates, mean ± SD). *P* values were determined by One-way ANOVA. **d** Src myristoylation in KYSE450 cells transfected with vector, ACSL4-flag, ACSL4-T679A-flag, and ACSL4-T679D-flag were analyzed by Click Chemistry, and detected by streptavidin-HRP. (**e**, left) Src/ERK pathway was detected after ACSL4 knock down. (**e**, right) Src/ERK pathway was detected after KYSE450 cells transfected with vector, ACSL4-flag, ACSL4-T679A-flag, and ACSL4-T679D-flag. **f** KYSE150 and KYSE70 cells were treated with 4NQO or heat stress to examine the change of p-p38 (T180/Y182), p-ACSL4 T679, and p-ERK1/2 (T202/Y204). **g** The samples were harvested and stained with IHC analysis of p-ACSL4 (T679) at different time points in 4NQO-induced ESCC progression ($n = 3$ biological replicates, mean ± SD). Statistical significance was conducted by two-sided unpaired Student's *t*-test. **h** KYSE150 and KYSE70 cells were subjected to SB202190 followed by treatment with heat stress and examined the change of p-p38 (T180/Y182), p-ACSL4 (T679), and p-ERK1/2 (T202/Y204) by Western blot. **i** Western blots on KYSE150 and KYSE70 cells with ACSL4 knockdown treated with LPS (p38 agonist) to observe the levels of p-p38 (T180/Y182), p-ACSL4 (T679), and p-ERK1/2 (T202/Y204). **j** p-p38, p-ACSL4 T679 and p-ERK1/2 (T202/Y204) was determined by Western blot in ACSL4 knockdown cells rescued with different ACSL4 T679 mutations. Representative immunoblots shown in figures were repeated three times independently with similar results. Source data are provided as a Source Data file.

models[48,49]. Moreover, persistent stress promotes cancer cell survival by evading apoptosis. This is achieved through the upregulation of BCL2 or caspase-3 mutation in tumor cells, which enables them to evade stress-induced apoptotic processes[48]. Additionally, prolonged stress also triggers anti-apoptotic signals via NF-κB activation or inhibition of p53-dependent apoptotic pathways through GSK3β activation[50]. Intriguingly, our results demonstrated that p38 signaling pathway termed stress-activated MAPKs medicated aberrant ERK1/2 proliferative signaling in ESCC process through ACSL4 activation (Figs. 1 and 2). There is evidence that high activity of p38 is recognized as a negative growth regulator by inhibition ERK[51]. Specifically, melanoma had simultaneously high activation ERK and p38 as well as there was a positive feedback loop to promote melanoma growth in vivo[52]. Similarly, high p38 activity contributes to the malignant phenotype of ESCC[53]. Moreover, our previous study also observed that p-p38 and p-ERK concurrently increased in ESCC tissue[45]. In this study, there was positive correlation between p-p38 and p-ERK under stress conditions, and our results demonstrated that stress pathway (p38) could directly activate growth pathway (Src-ERK) through ACSL4 medicated fatty acids (FA) metabolism.

ACSL4 is an essential enzyme for FA metabolism. ACSL4 dysregulation has been observed in various malignancies[54]. On the one hand, ACSL4 facilitates FA synthesis, thereby promoting the growth and metastasis of hepatoma cells[54,55]. Conversely, ACSL4 also catalyzes polyunsaturated fatty acids (PUFAs), especially arachidonic acid (AA) and adrenic acid (AdA), to AA-CoA or AdA-CoA, which transferred to the phospholipids of the plasma membrane, rendering them highly susceptible to peroxidation causing ferroptosis, which improved the response cancer immunotherapy in melanoma models[36,56–58]. Herein, we explored the function of ACSL4 in ESCC. ACSL4 presented higher expression in ESCC tissue compared to adjacent tissue and high ACSL4 was related with poor prognosis. Knockdown of ACSL4 inhibited cell

https://doi.org/10.1038/s41467-025-58342-z

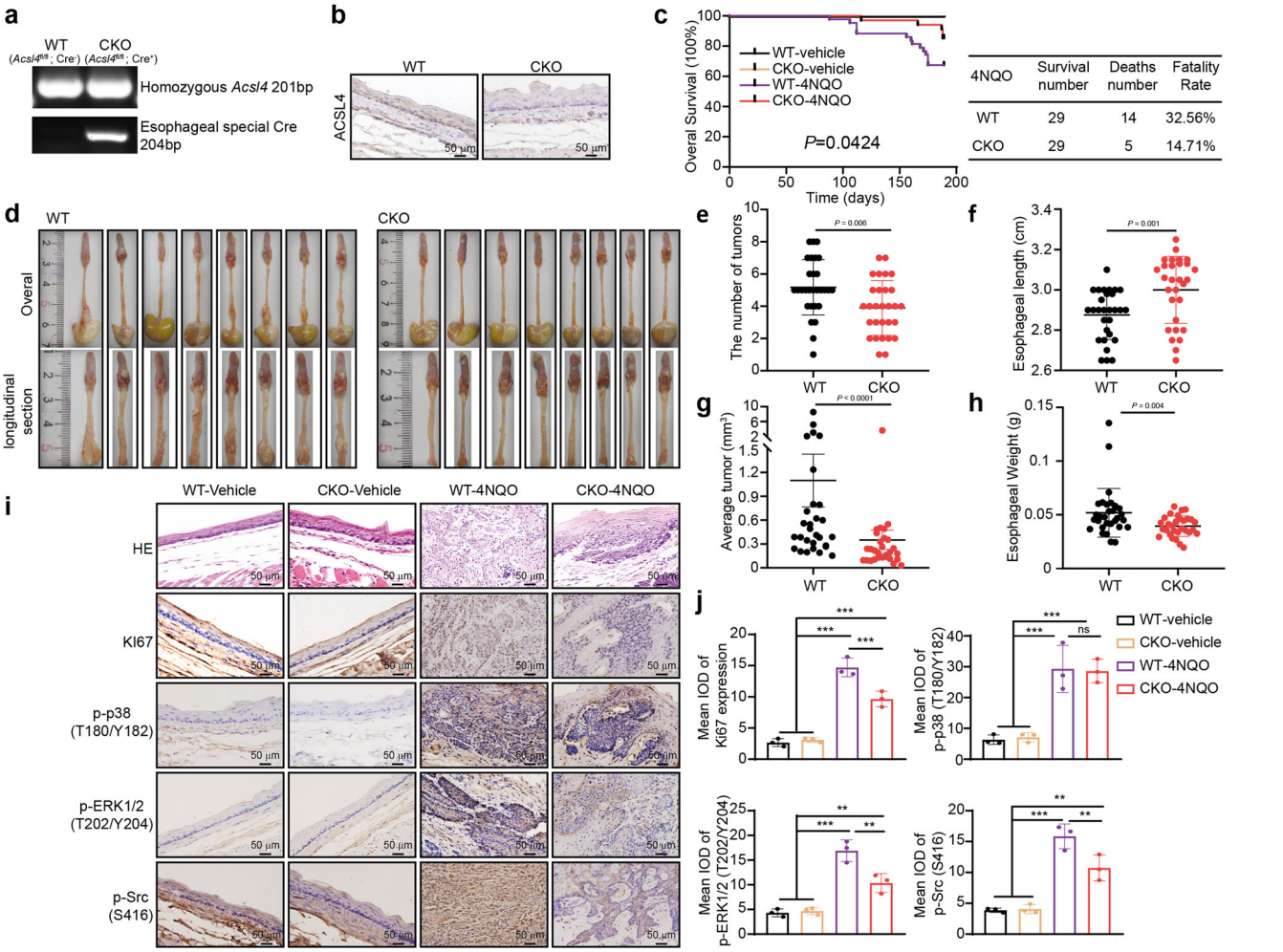

Fig. 6 | *Acsl4* knockout mouse deprived promoting-growth characteristic depending on p38/ACSL4/Src/ERK axis. a PCR genotyping was performed to distinguish between *Acsl4* wild-type (WT), and conditional knockout (CKO) mice. **b** IHC staining presents no ACSL4 expression in esophageal epithelium from CKO mice. **c** The mice survival of WT or CKO groups. *P* value was determined by Kaplan–Meier analysis. **d** Representative images of esophagus from mice. **e** The number of esophageal tumors was recorded. **f** The length of the esophageal in WT group and CKO group. **g** After esophageal dissection, the length and width of the tumor was measured using a digital caliper, and tumor volume was calculated using the formula volume = length (largest diameter) × width (perpendicular of "length") × width × 0.5[75]. Data were showed as mean values ± SEM. **h** The weight of esophagus was measured ($n = 29$ for each group). The data of (**e**, **f**, **h**) showed mean ± SD. Statistical significance of (**e**) was conducted by two-sided unpaired Student's *t*-test. *P* values of (**f**, **g** and **h**) were conducted by Mann–Whitney *U* test. **i** Esophageal samples were stained with H&E, Ki-67, p-p38 (T180/Y182), p-ERK1/2 (T202/Y204), and p-Src (S416) in different groups. **j** Protein levels of Ki-67, p-p38 (T180/Y182), p-ERK1/2 (T202/Y204), and p-Src S416 were analyzed ($n = 3$ samples detected from 3 independent mice, Mean ± SD). *P* values were determined by One-way ANOVA. For Ki67 expression: WT-vehicle vs WT-4NQO, *** $P < 0.0001$; WT-vehicle vs CKO-4NQO, *** $P < 0.0001$; CKO-vehicle vs WT-4NQO, *** $P < 0.0001$; CKO-vehicle vs CKO-4NQO, *** $P < 0.0001$; WT-4NQOvs CKO-4NQO, *** $P = 0.000354$. For p-p38(T180/Y182): WT-vehicle vs WT-4NQO, *** $P = 0.000216$; WT-vehicle vs CKO-4NQO, *** $P = 0.000265$; CKO-vehicle vs WT-4NQO, *** $P = 0.000272$; CKO-vehicle vs CKO-4NQO, *** $P = 0.000335$; WT-4NQO vs CKO-4NQO, ns $P = 0.854$. For p-ERK1/2(T202/Y204): WT-vehicle vs WT-4NQO, *** $P < 0.0001$; WT-vehicle vs CKO-4NQO, ** $P = 0.001$; CKO-vehicle vs WT-4NQO, *** $P < 0.0001$; CKO-vehicle vs CKO-4NQO, ** $P = 0.002$; WT-4NQO vs CKO-4NQO, ** $P = 0.001$. For p-SRC (S416): WT-vehicle vs WT-4NQO, *** $P < 0.0001$; WT-vehicle vs CKO-4NQO, ** $P = 0.001$; CKO-vehicle vs WT-4NQO, *** $P < 0.0001$; CKO-vehicle vs CKO-4NQO, ** $P = 0.001$; WT-4NQO vs CKO-4NQO, ** $P = 0.003$. Source data are provided as a Source Data file.

growth in vitro and in vivo (Figs. 3 and 4). These data provide the strong evidence that the potent oncogenic and tumor-promoting activity of ACSL4 in ESCC.

Previous studies indicate that phosphorylation of ACSL4 by PKC is essential for ferroptosis[36,59]. Nevertheless, whether the phosphorylation site of ACSL4 affects enzyme activity or ACSL4 is responsible for regulating cancer cell proliferation dependent on enzyme activity has not been fully elucidated. Our findings identified the T679 site played a crucial role for ACSL4 enzyme activation and oncogenic function (Fig. 4j–p). We also found that p38 directly bound to ACSL4 and phosphorylation at T679 (Fig. 2), further induced enzyme activity to generate more C14:0 CoA (Fig. 5c). Acyl-CoA forms produced by ACSL family not only serve as ingredient in metabolic pathways but also participate in protein acylation to maintain activity via corresponding transferase[60]. The myristoylation is described as a process where myristoyl-CoA binds with N-myristoyl transferas, delivering myristate to the protein while releasing CoA[61]. Myristoylation protein utilize the motif to attach to the membrane, which is required for their function, such as c-Src[62]. ACSL4 has been reported to regulate myristoylation protein in prostate cancer cells[28], but the precise mechanism has not been determined. We identified that phosphorylation ACSL4 at T679 by p38 catalyzed an increased production of C14:0 CoA, which is subsequently transferred to Src to simulate Src/MAPK/ERK pathway to facilitate cell proliferation. Additionally, ACSL4 knock down impaired Src myristoylation to further impaired Src-ERK signaling pathway whereas introduction of T679D could promote the yield of Src

myristoylation to promote the pathway (Fig. 5b–e). Due to the functional similarities among the ACSL family members, it's essential to exclude the role of other members on Src myristoylation for ESCC development. Of note, ACSL4 exhibited increase at both mRNA level and protein level. Although ACSL1 has been reported to improve FSP1 myristoylation[63], this study indicated that Src myristoylation presented a notable inhibition upon ACSL4 knock down. Nevertheless, other members of the family showed limited effect possibly due to relatively low expression (Supplemental Fig. 4).

Further, we established the mice model by 4NQO with similar pathological morphology of human ESCC process[64,65]. With disease progresses upon chronic stress, p-p38 (T180/Y182), p-ERK (T202/Y204), and p-ACSL4 (T679) gradually increased. Due to knockout *Acsl4* results in embryonic lethality[26,66,67] and to better present the essential role in ESCC development, we established mice with deletion *Acsl4* in esophagus. Mice with *Acsl4* knockout were deprived promoting-growth characteristic depending on p38/ACSL4/Src/ERK axis, and presented better survival time with lower tumor burden (Fig. 6). Although *Acsl4* gene is located X- chromosome, female mice showed no sensitivity to ESCC than male group. This suggests that there may be no significant gender-based variation in ACSL4 protein expression due to the X-inactivation mechanism[68]. This report documents an inherent connection between external stimuli response pathway and cancer cell proliferation via ACSL4 phosphorylation to collect C14:0 CoA.

In summary, our data indicate the intriguing mechanism of stress promoting tumor growth through ACSL4 mediating generation more myristoyl-CoA to modify Src. We demonstrate that the p38/ACSL4/Src/ERK axis facilitates activation of external triggers and subsequent growth pathway leading to tumor development. In-depth study of this pathway may offer potential targets and strategies for ESCC prevention and therapy (Fig. 7).

Methods

Cell culture

Human ESCC cell lines including KYSE150, KYSE70, and KYSE450, human normal esophageal epithelium cell line HET-1A, HEK293T cell line and HEK293F cells were preserved and donated by Professor Ziming Dong (the Department of Pathophysiology, school of basic medical sciences of Zhengzhou University)[69–71]. These cell lines were cytogenetically tested by STR authenticated and were confirmed to be mycoplasma-free. Subsequently, ESCC cell lines were cultured in 1640 medium (Biological Industries) containing 10% fetal bovine serum (FBS) (VivaCell). HET-1A and HEK293T cells were cultured in DMEM medium (Biological Industries) with 10% FBS. HEK293F cells were serum-free medium 293T-II (Sino Biological Inc.). These cells were incubated at 37 °C with 5% CO_2 humidified atmosphere.

Antibodies and reagents

Antibodies specific to GAPDH (ZSGB-BIO, TA-08, 1:3000 for WB), β-Tubulin (ZSGB-BIO, TA-10 1:3000 for WB), β-Tubulin (HUABIO, EM0103 1:5000 for WB) p-AKT S473 (CST, 4060S, 1:1000 for WB), p-p38 (T180/Y182) (CST, 9211S, 1:1000 for WB, 1:100 for IHC), p-ERK1/2 (Thr202/Tyr204) (CST,4370S, 1:2000 for WB, 1:200 for IHC), p-STAT3 S727 (CST, 9134S, 1:1000 for WB), p-JNK2 (T183/Y185) (CST, 4668S, 1:1000 for WB), T-AKT (CST, 9272S, 1:1000 for WB), T-p38 (CST, 9212S, 1:1000 for WB), T-p38 (abcam, ab170099, 1:50 for IP), T-ERK1/2 (CST, 4695S, 1:1000 for WB), T-JNK (CST, 9252S, 1:1000 for WB), Ki67 (Servicebio, GB151499-100, 1:400 for IHC), Flag-tag (MBL, M185-3MS, 1:50 for IP, 1:10000 for WB), V5-tag (CST, 13202S, 1:1000 for WB, 1:50 for IP), HA-tag (Santa cruz, sc-7392, 1:100 for IP, 1:1000 for WB), GST-tag (Santa cruz, sc-138, 1:1000 for WB), normal mouse IgG (Santa cruz, sc-2025, 1:100 for IP), normal rabbit IgG (CST, 2729S, 1:100 for IP), ACSL4 (proteintech, 1:2000 for WB, 1:100 for IHC), ACSL4 (Santa cruz, sc-365230, 1:250 for IP), p-ACSL4 (Biolynx, AB007346-1, 1:500 for WB, 1:200 for IHC), T-SRC (CST, 2108S, 1:1000 for WB), p-SRC S416 (CST, 6943S, 1:1000 for WB), p-SRC S416 (Gene Tex, GTX24816, 1:100 for IHC), HSPA1A (Santa cruz, sc-59569, 1:500 for WB), HSP9β (Abcam, ab203085, 1:1000 for WB), HSPA8 (CUSABIO, CSB-PA03249A0Rb, 1:1000 for WB), ACSL1 (Huabio, HA601112, 1:1000 for WB), ACSL3 (Proteintech, 20710-1-AP, 1:1000 for WB), ACSL5 (Proteintech, 15708-1-AP, 1:1000 for WB), ACSL6 (CUSABIO, CSB-PA892139LA01HU, 1:500 for WB), Goat anti-rabbit IgG H & L (HRP) (ZSGB-Bio, ZB2306, 1:5000 for WB), Goat anti-mouse IgG H & L (HRP) (ZSGB-Bio, ZB2305, 1:5000 for WB) were dissolved in 5% BSA (Solarbio) and kept at −20 °C. Thr679-ACSL4 phosphorylation-specific antibody p-ACSL4 (Thr679) was ordered and produced by BioLynx Technology, and the sequence is CRLSPEPWTPETGLVT.

SB202190 (MedChemExpress, HY-10295), SP600125 (GLPBIO, GC15344), AZD1480 (GLPBIO, GC12504), SCH772984(GLPBIO, GC16001), Doramapimod (Selleck, S1574) and Saracatinib (MedChemExpress, HY-10234), LPS (Sigma-Aldrich, L2630), 4NQO (Energy Chemical, E031787).

MTT assay, colony formation and soft agar assay

The cells (1×10^4/mL) were seeded in 96-well plates and incubation for 16 h. Subsequently, cells were treated with MTT (0.5 μg/mL) agents for 2 h at different time points to test cell growth. For the colony formation assay, cells (300 per well) were seeded in 6-well plates and incubated for 7 days. Afterward, the colonies were treated with 4% paraformaldehyde for 30 min at room temperature (RT) and followed by staining with crystal violet for 30 min at RT. Finally, the colonies were photographed using BIORAD imaging system. For soft agar assay, cells (8×10^3/well) were suspended in 2 × BME medium (Sigma-Aldrich, B9638) were mixed with 0.33% agar (BD biosciences, 214050) and 10% FBS. Then, the cells were cultured at 37 °C in an incubator with 5% CO_2 for 10 days. Finally, the colonies were visualized and counted by IN Cell Analysis 6000.

Animal experiments

SCID/cb17 female mice (6–7 weeks) were obtained from Vital River Laboratory Animal Technology (Beijing). C57BL/6 mice (6–7 weeks) were acquired from The Animal Experimental Center of Zhengzhou University. Mice were kept in a specific pathogen-free (SPF) environment, subjected to a 12-h light/12-h dark cycle. The room temperature was controlled at 20 °C ± 2 with 60% humidity. Mice had free access to water and rodent diet (Beijing keao xieli feed co., LTD, 1016706476803973120). This study was approved by the Research Ethics Committee of Zhengzhou University. All animal procedures in this study were approved by the Zhengzhou University Institutional Animal Care and Use Committee (ZZUIRB2022-70).

Cell-derived xenograft mouse model

KYSE150 cell stably transfected PLKO.1 were used as a mock control, and KYSE150 ACSL4 shRNA cells were resuspended in cold-PBS with 1‰ penicillin-streptomycin. KYSE150 (5×10^6), KYSE70 (7×10^6) or KYSE450 (1×10^7) cells were subcutaneously injected into the flank of SCID/cb17 female mice. Mice were randomly divided into mock, sh-1, and sh-5 group. The volume of tumor mass was recorded twice a week. Once average volume of tumors in mock group reached 1000 mm^3, mice were offered euthanasia. Maximum tumor size is 2000 mm^3 according to the Animal Ethics Committee. Notably, the maximal tumor burden didn't exceed the limitation in this study. In CDX models, we used 6–7 weeks old female SCID/cb17 mice. The model is used to evaluate the tumorigenesis of the cells without special requirement for gender. Therefore, we used females with a more moderate character. Tumor volume was counted using the formula: length × width × width × 0.5.

4NQO-induced multi-stage ESCC development

C57BL/6 mice (8 weeks old) were subjected to a 16-weeks treatment with 100 μg/mL 4NQO in water. Mice were randomly divided into

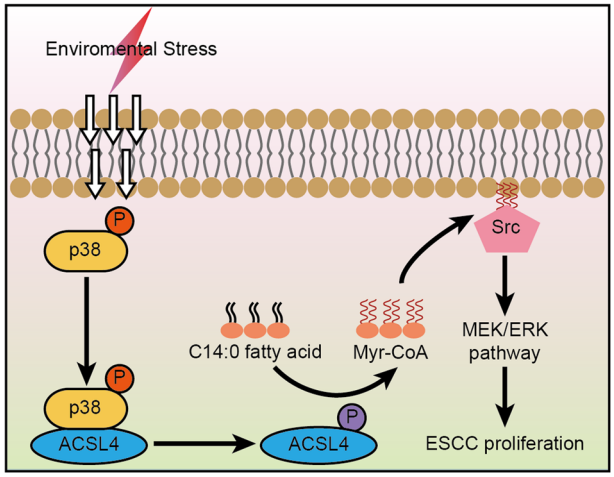

Fig. 7 | Proposed model for p38 phosphorylation of ACSL4 to promote Src myristoylation and ESCC progression via Src/ERK pathway. Environmental stress leads to p38 activation. Activated p38 binds ACSL4 and phosphorylates ACSL4 at T679 site, which in turn activates ACSL4, triggering production of C14:0 CoA and then promoting Src myristoylation. Myristoylation modification is required for function of Src, which facilitates Src-ERK pathway activation. Finally, p38-ACSL4-Src-ERK pathway launches ESCC tumorigenesis and progression. Created by Adobe Illustrator.

water and 4NQO treatment group. The drinking water containing 4NQO was kept in light-shielded bottles and maintained freshly prepared once a week. Following the completion of the 16 weeks treatment, fresh sterile water (10 weeks) was replaced to 4NQO drinking water until mice were offered euthanasia. The weights of mice were monitored every two weeks. After a total duration of 26 weeks, the entire esophagus and tongues were excised for subsequent measurements, including esophageal length, tumor numbers, and tumor volumes. Each esophagus was cut into two parts, and one part was stored at −80 °C while the other part was kept in formalin for hematoxylin-eosin (H&E) staining.

Subsequently, two independent pathologists conducted the histological determination of the esophageal lesions according to criteria described previously[65,72]. 4NQO-induced multi-stage ESCC development. Normal (NOR) represents normal esophageal epithelial tissue, showing a well-oriented arrangement of cells with the basal layer about one to two cells thick. Inflammation (INF) stage still maintains normal epithelium but infiltration by inflammatory cells including neutrophils, lymphocytes or eosinophils. Stage hyperplasia (HYP) usually shows a slight thickness and disorder of basal zone, and these abnormalities are limited in the lower third of the epithelium. Stage dysplasia (DYS) presents nuclear atypia including enlargement, hyperchromatic, pleomorphism, meanwhile loss of normal cell polarity, and abnormal tissue maturation were confined to lower two thirds of the epithelium. When dysplastic squamous cells involve the full thickness of the epithelium, it is named carcinoma in situ (CIS) stage. In invasive carcinoma (ICA) stage, neoplastic squamous cells invade into the basement membrane.

Image j pro plus software was used to analyze the IHC images, and the mean IOD (intensity of DAB) of positive cells in each image was recorded. For NOR and INF tissues, the basal layer part was circled and counted. For HYP and DYS, the epithelial cells with loss of polarity, basal cell hyperplasia, disordered, and nuclear pleomorphism were analyzed. For CIS and ICA, full epithelial layer or the tissue with pathological changes of cancer were counted.

4NQO-induced esophageal cancer in wild-type (WT) and esophagus conditional *Acsl4*-knockout mice (*Acsl4*-CKO)

Homozygous C57BL/6J mice ($Acsl4^{fl/fl}$, 1 male, 6 weeks) and heterozygous C57BL/6 J mice ($Acsl4^{fl/+}$, 2 females, 6 weeks) were purchased from Cyagen Biosciences Inc. ED-L2-Cre mice (6 weeks) were purchased from Vitalstar Biotechnology Co., Ltd. $Acsl4^{fl/fl}$ and $Acsl4^{fl/+}$ mice were mated with ED-L2-Cre mice to create $Acsl4^{fl/fl,\ Cre+}$ mice. $Acsl4^{fl/fl,\ Cre+}$ mice were defined as *Acsl4*-CKO, and $Acsl4^{fl/fl}$ mice served as the control group (WT). After reproduction, DNA from the tails of the mice was extracted and confirmed by PCR assay. WT ($n = 43$) and *Acsl4*-CKO ($n = 34$) mice were included in the experiment. The whole procedure of 4NQO-induced esophageal cancer is the same as above. We used 6–8 weeks old female and male C57BL/6 mice. WT-vehicle: 3 female, 3 male; CKO--vehicle: 3 female, 3 male; WT-4NQO: 16 female, 27 male; CKO-4NQO: 12 female, 22 male.

Western blot

HET-1A, KYSE150, and KYSE70 cells were cultured in 6 cm dishes, and treatment with different inhibitors respectively for 2 h following by 50 μM 4NQO exposure or maintained at 42 °C at different time points. After washing twice with pre-chilled PBS, cells were incubated on ice for 30 min with RIPA lysis buffer supplemented with protease inhibitors and 100 μM PMSF. Following centrifugation (13,000 × *g*, 30 min), the protein was collected and the concentration was determined using BCA kit (Beyotime Biotechnology, P0011). Equal amounts of protein samples were separated by 10% SDS-PAGE and then transferred to a PVDF membrane at 90 V for 2 h. After being blocked, the membranes were incubated at 4 °C overnight with specific primary antibodies. The secondary antibody was incubated for another 2 h at RT. The protein bands were visualized with chemiluminescent kit (MeilunBio). Finally, Quantification of Western blots were carried out by the ImageJ software. Written informed consent was provided by all patients for the use of tissue samples.

And the siRNA sequences were shown in "Supplementary Table 1". RNAi were produced by Sangon Biotech (Shanghai) Co., Ltd.

IP/ mass spectrometry (MS) analysis and Co-Immunoprecipitation

HEK293T cells were transfected with PLVX-p38-3 × Flag or vector as control group for 36 h and collected cell lysate using NP-40 lysis buffer. The cell lysates (1 mg) were incubated with 20 μL of protein A/G agarose beads (Santa Cruz) for 2 h. The supernatant and 1 μg Flag antibody were mixed with 40 μL of protein A/G agarose beads at 4 °C for 4 h. The p38-Flag beads complex was incubated with KYSE150 cell lysis (1 mg) at 4 °C for 4 h. After the beads were washed three times using NP-40 lysis buffer, the samples were subjected to SDS/PAGE. Using silver staining (Beyotime Biotechnology, P0017S), the gel lanes were cut down separately and prepared for mass spectrometry.

Maxquant (1.6.1.0) was used for mass spectrometry analysis and resulting sequences were searched against uniprot database (Homo_sapiens_207393_2023223.fasta) with mass error tolerances of 6 ppm for parent and 20 ppm for fragment ions. Trypsin was used for digestion allowed for a maximum of two missed cleavages. Carbamidomethyl was set as fixed modification, whereas oxidation was defined as variable modifications for database searching. FDR was set as <0.01 at the peptide-spectrum match level.

HEK293T cells were transfected with Flag-ACSL4 or V5-p38 plasmids or both. After 36 h, cells were collected and homogenized in NP-40 lysis buffer containing phosphatase or protease inhibitors. Lysate containing 1 mg protein was preliminarily cleaned with 20 μL of protein A/G agarose beads for 2 h. Subsequently, the supernatant was incubated overnight at 4 °C with 1 μg primary antibody (anti-Flag or anti-V5) and 40 μL beads after centrifugation. The sample was resolved by SDS-PAGE gel followed by the precipitates after being washed with lysis buffer and boiled in 50 μL 3 × loading buffer.

Fatty acyl-CoA analysis by LC-MS/MS

The method for extraction and analysis of long chain fatty acyl-CoAs from biological samples was described previously[73]. The ESCC cells

(KYSE150, KYSE70 and KYSE450) were treated with 400 μM myristic acid (Sigma, M3128) in 1640 medium including 2% fatty acid free BSA (Equitrch-Bio Inc., BAH66) for 24 h. Subsequently, the cells were collected after being washed with PBS. The sediment was then incubated with 15 μL 10 μM C15:0 CoA (acting as internal standard, ISTD) at −80 °C for 15 min in 2 mL methanol. After centrifugation at 15,000 × *g* and 4 °C for 10 min, the supernatant was transferred into a new glass tube and then mixed with 1 mL acetonitrile. The sample was evaporated at 55 °C for 30 min in a vacuum concentrator. The sample was resuspended in 150 μL methanol, and then centrifuged at 15,000 × *g* for 10 min at 4 °C after vortexing. Finally, 100 μL supernatant was collected into an autosampler vial for subsequent analysis. The results were normalized to whole cell protein and were shown as pmol/mg protein.

Quantitation. C14:0 CoA (sigma, 870714P) and C15:0 CoA (sigma, 870715 P) as ISTD was mixed as reference standard for calibration samples with a final concentration of 0.25, 0.5, 1, 2.5, 5, 10, 25, 50 μM. The peak area for analyte associating with the amount of acyl-CoA was used to a calibration curve. Slopes (k) of the linear regression from calibration curve of C14:0 CoA and C15:0 CoA were calculated respectively, and the ratio of slopes (R) = k (C14:0 CoA)/k (C15:0 CoA) was calculated. Meanwhile, the power of R (1/R) was recorded. The sample with 150 pmol C15:0 CoA, and the amount of C14:0 CoA could be determined upon signal-to-noise ratio exceeds 10. The detailed formula as follows:

$$\text{Response ratio} = \text{Peak area}(C14:0\,\text{CoA})/\text{Peak area}(C15:0\text{CoA})$$

$$C14:0\text{CoA} = 150(\text{pmol}) \times \text{response ratio} \times (1/R)$$

Except for the number of cells causing the differences in samples, the quantification C14:0 CoA was recorded as pmol/mg.

LC-MS/MS conditions

SHIMADZU LC-30A/AB SCIEX Triple Quad TM 4500 LC-MS/MS was employed for analysis, and Waters BEH C18 column (2.1 × 100 mm, 1.7 μm) was utilized for analyte separation. The volume of injected solution was 5 μL. The mobile phase A was 10 mM ammonium acetate (pH 6.8) and the mobile phase B was acetonitrile. Analytes were separated using a gradient method, with a 0.3 mL/min flow rate, (time/minute, % mobile phase B): (0, 65), (1, 99), (4, 99), (4.1, 65), and the run time for each injection was 6 min. Analyst 1.6.2 software was used to collect the data, and MultiQuant 2.1.1 software by SCEIX was applied for data processing.

Click chemistry

Click chemistry analysis was performed as previously described[28]. KYSE150 and KYSE70 cells transduced with shRNA-control, shACSL4#1 or shACSL4#5 were cultured in 1640 medium with 2% fatty acid free BSA and treatment with 400 μM alkynyl-myristic acid (GLPBIO) for 24 h. The protein lysates were extracted using PBS containing 1% NP-40 and protease inhibitors. Subsequently, 40 μL A/G beads were mixed with 1 mg of cell lysates and incubated at 4 °C for 2 h with gentle rotation. After centrifuge (2500 × *g* for 5 min), cell lysates were collected and were incubated with 1 μg Src antibody and 40 μL A/G beads overnight at 4 °C. After three times washing with PBS, the supernatant was discarded and the beads combination with Src was subjected to the Click chemistry reaction in Click reaction buffer (2 mM CuSO4, 1 mM bis(tert-butyl)-tris (triazolylmethyl) amine-propanol, 10 mM sodium L-ascorbate, 100 μM biotin-azide) at 30 °C for 1 h. Finally, 30 μL 6 × loading buffer was added, and the samples were heated for 5 min at 100 °C and resolved by SDS-PAGE gel. The myristoylation of Src was biotinylated and specifically recognized by the Streptavidin-HRP antibody.

In vitro kinase assay

The ACSL4-GST plasmid was constructed for protein expression in *Escherichia coli*. Human recombinant ACSL4-GST or ACSL4-T679A-GST (1000 ng) was mixed with or without (negative controls) human recombinant activated 200 ng of p38α kinase (Signal chem) in 1 × kinase buffer containing 2 mM DTT and 200 μM ATP, followed by incubation at 30 °C for 30 min. To terminate the kinase reaction, 30 μL of 6 × SDS loading buffer was added into each sample. The phosphorylation status of Thr residue on ACSL4 was assessed using both the pan-Thr and p-ACSL4 (T679) antibody.

GST pull down assay

The GST and ACSL4-GST proteins were expressed in *Escherichia coli* and purified using 10 mM GSH. p38-3 × flag fusion protein was expressed in HEK293F cells and purified with 150 ng/μL 3 × flag peptide. ACSL4 or GST fusion protein was incubated with glutathione sepharose 4B at 4 °C for 3 h. After washing the beads three times with PBS, the p38 fusion protein was added and mixed, the mixture was incubated overnight at 4 °C. Subsequently, the samples were resolved by SDS-PAGE gel.

Lentiviral infection and transfection

The HEK293T cells were seeded in 6 cm dish and cultured until they reached approximately 60% confluence. Subsequently, packaging vectors including psPAX2, pMD2.G and every viral vector (sh-PLKO.1, sh-ACSL4#1, sh-ACSL4#5, pLVX-ACSL4, pLVX-ACSL4-T679A, pLVX-ACSL4-T679D and sg-ACSL4#3) were mixed at a mass ratio of 1:3:4 using Jet Primer and transfected into HEK293T cells. The viral particles were collected and filtered using 0.45 μm filter followed by 48 h transfection. The KYSE150, KYSE70 and KYSE450 cells were infected with relevant virus particles supplemented with 8 μg/mL polybrene (Solarbio) upon reaching 60% confluence in a 10 cm dish. After 24 h infection, cell selection was performed using 2 μg/mL puromycin (Solarbio). The shRNA and sgRNA sequences were shown in "Supplementary Table 2". The shRNA and sgRNA sequences were produced by Sangon Biotech (Shanghai) Co., Ltd.

Computer docking model

The crystal structure of p38 was downloaded from PDB database (PDB: 5xyy), while structure of ACSL4 (AF-O060488) was predicted by Alphafold v2.0. Alphafold was used for docking simulation.

Immunohistochemistry (IHC)

IHC assay was performed as previously described[74]. All specimens were fixed on slides with 4 μm-thick tissue sections, and subjected to xylene, various concentrations of ethanol (100%-100%-90%-80%-50%), and 1 × TBST. Antigen retrieval was performed in tris-EDTA buffer (pH 9.0) or citrate buffer (pH 6.0) for 3 min using heat. After treatment with 3% H_2O_2 for 5 min, the tissues were incubated with specific primary antibodies at 4 °C overnight. Then, the secondary antibody was added to the slides for 30 min at 37 °C followed by washing 3 times with 1 × TBST. Diaminobenzidine (DAB) was used to stain and hematoxylin was performed to counterstain for cell nucleus. Finally, Image-Pro Plus software was performed to count the mean IOD of positive cells. For precancerous lesions, we focus on the epithelial cells with loss of polarity, basal cell hyperplasia, disordered, and nuclear pleomorphism. Images were obtained by the microscope (Olympus) and the resolution of the images was 300 dpi.

Quantitative real-time PCR (qRT-PCR)

Total RNA was extracted with TRIzon reagent (CWBIO, CW0580S) and reversed to cDNA using Primer Script reverse transcription reagent kit

(Takara, 6210 A). The cDNA samples were mixed with TB Green® Fast qPCR Mix (Takara, RR820A) and analyzed on CFX96 real-time PCR Detection System (Bio-RAD). GAPDH was served as the reference transcript. The relative mRNA expression was performed using $2^{(-\Delta\Delta CT)}$ method. Primer sequences were listed in "Supplementary Table 3". Primer sequences were produced by Sangon Biotech (Shanghai) Co., Ltd.

Statistical analysis

All results in the study are represented as mean ± SD. Two-tailed unpaired Student's *t* test was conducted for comparison of means of data between two groups. One-way ANOVA was used to compare multiple independent groups. Nonparametric tests (Mann–Whitney *U* test) was used to detect difference when the data distribution is not normally distribution. SPSS 22.0 was used for statistical analysis. $P < 0.05$ was recognized as statistically significant.

Illustrations

In the Figs. 1c, 2a and 7, all of elements were created using Created by Adobe Illustrator (Adobe Inc, Adobe Illustrator 2020).

Reporting summary

Further information on research design is available in the Nature Portfolio Reporting Summary linked to this article.

Data availability

The mass spectrometry proteomics data in this study have been deposited to the ProteomeXchange Consortium via the PRIDE partner repository under accession code PXD053908. GSE23400 and GSE44021 were download on the GEO database. The pictures of Fig. 3b and Supplemental Fig. 4a were download from GEPIA database (http://gepia.cancer-pku.cn/). And the parameters were set as: gene symbol, ACSL4/ACSL1/ACSL3/ACSL5; |log2FC|, 1; *P* value, 0.01; Jitter size, 0.4. The remaining data are available within the Article, Supplementary Information or Source Data file. Source data are provided with this paper.

References

1. Galluzzi, L., Yamazaki, T. & Kroemer, G. Linking cellular stress responses to systemic homeostasis. *Nat. Rev. Mol. Cell Biol.* **19**, 731–745 (2018).
2. Derks, K. W., Hoeijmakers, J. H. & Pothof, J. The DNA damage response: the omics era and its impact. *DNA Repair (Amst.)* **19**, 214–220 (2014).
3. Fasano, C., Disciglio, V., Bertora, S., Lepore Signorile, M. & Simone, C. FOXO3a from the nucleus to the mitochondria: a round trip in cellular stress response. *Cells* **8**, https://doi.org/10.3390/cells8091110 (2019).
4. Han, J., Wu, J. & Silke, J. An overview of mammalian p38 mitogen-activated protein kinases, central regulators of cell stress and receptor signaling. *F1000Res.* **9**, https://doi.org/10.12688/f1000research.22092.1 (2020).
5. Theodosiou, A. & Ashworth, A. Differential effects of stress stimuli on a JNK-inactivating phosphatase. *Oncogene* **21**, 2387–2397 (2002).
6. McGrail, D. J. et al. Defective replication stress response is inherently linked to the cancer stem cell phenotype. *Cell Rep.* **23**, 2095–2106 (2018).
7. Groelly, F. J., Fawkes, M., Dagg, R. A., Blackford, A. N. & Tarsounas, M. Targeting DNA damage response pathways in cancer. *Nat. Rev. Cancer* **23**, 78–94 (2023).
8. Oakes, S. A. & Papa, F. R. The role of endoplasmic reticulum stress in human pathology. *Annu. Rev. Pathol.* **10**, 173–194 (2015).
9. Urra, H., Dufey, E., Avril, T., Chevet, E. & Hetz, C. Endoplasmic reticulum stress and the hallmarks of cancer. *Trends Cancer* **2**, 252–262 (2016).
10. Lim, D. Y. et al. (+)-2-(1-Hydroxyl-4-oxocyclohexyl) ethyl caffeate suppresses solar UV-induced skin carcinogenesis by targeting PI3K, ERK1/2, and p38. *Cancer Prev. Res. (Philos.)* **7**, 856–865 (2014).
11. Liu, K. et al. Sunlight UV-induced skin cancer relies upon activation of the p38alpha signaling pathway. *Cancer Res.* **73**, 2181–2188 (2013).
12. Insua-Rodriguez, J. et al. Stress signaling in breast cancer cells induces matrix components that promote chemoresistant metastasis. *EMBO Mol. Med.* **10**, https://doi.org/10.15252/emmm.201809003 (2018).
13. Chiba, T., Marusawa, H. & Ushijima, T. Inflammation-associated cancer development in digestive organs: mechanisms and roles for genetic and epigenetic modulation. *Gastroenterology* **143**, 550–563 (2012).
14. Shah, S. C. & Itzkowitz, S. H. Colorectal cancer in inflammatory bowel disease: mechanisms and management. *Gastroenterology* **162**, 715–730 e713 (2022).
15. Akiyama, S. et al. Prognostic impact of MutT homolog-1 expression on esophageal squamous cell carcinoma. *Cancer Med.* **6**, 258–266 (2017).
16. Murata, M. Inflammation and cancer. *Environ. Health Prev. Med.* **23**, 50 (2018).
17. Camargo, M. C. et al. Associations of circulating mediators of inflammation, cell regulation and immune response with esophageal squamous cell carcinoma. *J. Cancer Res. Clin. Oncol.* **147**, 2885–2892 (2021).
18. Chen, J. et al. The diacylglycerol kinase alpha (DGKalpha)/Akt/NF-kappaB feedforward loop promotes esophageal squamous cell carcinoma (ESCC) progression via FAK-dependent and FAK-independent manner. *Oncogene* **38**, 2533–2550 (2019).
19. Abnet, C. C., Arnold, M. & Wei, W. Q. Epidemiology of esophageal squamous cell carcinoma. *Gastroenterology* **154**, 360–373 (2018).
20. Maghsudlu, M. & Farashahi Yazd, E. Heat-induced inflammation and its role in esophageal cancer. *J. Dig. Dis.* **18**, 431–444 (2017).
21. Faubert, B., Solmonson, A. & DeBerardinis, R. J. Metabolic reprogramming and cancer progression. *Science* **368**, https://doi.org/10.1126/science.aaw5473 (2020).
22. Vriens, K. et al. Evidence for an alternative fatty acid desaturation pathway increasing cancer plasticity. *Nature* **566**, 403–406 (2019).
23. Hoy, A. J., Nagarajan, S. R. & Butler, L. M. Tumour fatty acid metabolism in the context of therapy resistance and obesity. *Nat. Rev. Cancer* **21**, 753–766 (2021).
24. Rossi Sebastiano, M. & Konstantinidou, G. Targeting long chain Acyl-CoA synthetases for cancer therapy. *Int. J. Mol. Sci.* **20**, https://doi.org/10.3390/ijms20153624 (2019).
25. Kuwata, H. et al. Long-chain acyl-CoA synthetase 4 participates in the formation of highly unsaturated fatty acid-containing phospholipids in murine macrophages. *Biochim. Biophys. Acta Mol. Cell Biol. Lipids* **1864**, 1606–1618 (2019).
26. Meloni, I. et al. FACL4, encoding fatty acid-CoA ligase 4, is mutated in nonspecific X-linked mental retardation. *Nat. Genet.* **30**, 436–440 (2002).
27. Hou, J. et al. ACSL4 as a potential target and biomarker for anticancer: from molecular mechanisms to clinical therapeutics. *Front. Pharm.* **13**, 949863 (2022).
28. Ma, Y. et al. Long-Chain Acyl-CoA synthetase 4-mediated fatty acid metabolism sustains androgen receptor pathway-independent prostate cancer. *Mol. Cancer Res.* **19**, 124–135 (2021).
29. Li, Y. J. et al. Fatty acid oxidation protects cancer cells from apoptosis by increasing mitochondrial membrane lipids. *Cell Rep.* **39**, 110870 (2022).

30. Cheng, J. et al. ACSL4 suppresses glioma cells proliferation via activating ferroptosis. *Oncol. Rep.* **43**, 147–158 (2020).
31. Feng, J. et al. ACSL4 is a predictive biomarker of sorafenib sensitivity in hepatocellular carcinoma. *Acta Pharm. Sin.* **42**, 160–170 (2021).
32. Li, J. et al. Norathyriol suppresses skin cancers induced by solar ultraviolet radiation by targeting ERK kinases. *Cancer Res.* **72**, 260–270 (2012).
33. Gong, X. et al. Stress-induced interaction between p38 MAPK and HSP70. *Biochem. Biophys. Res. Commun.* **425**, 357–362 (2012).
34. Sun, P. et al. Hsp90 modulates human sperm capacitation via the Erk1/2 and p38 MAPK signaling pathways. *Reprod. Biol. Endocrinol.* **19**, 39 (2021).
35. Trempolec, N., Dave-Coll, N. & Nebreda, A. R. SnapShot: p38 MAPK substrates. *Cell* **152**, 924–924 e921 (2013).
36. Zhang, H. L. et al. PKCbetaII phosphorylates ACSL4 to amplify lipid peroxidation to induce ferroptosis. *Nat. Cell Biol.* **24**, 88–98 (2022).
37. Soupene, E. & Kuypers, F. A. Mammalian long-chain acyl-CoA synthetases. *Exp. Biol. Med. (Maywood)* **233**, 507–521 (2008).
38. Patwardhan, P. & Resh, M. D. Myristoylation and membrane binding regulate c-Src stability and kinase activity. *Mol. Cell Biol.* **30**, 4094–4107 (2010).
39. Zhang, X. et al. Src acts as the target of matrine to inhibit the proliferation of cancer cells by regulating phosphorylation signaling pathways. *Cell Death Dis.* **12**, 931 (2021).
40. Jin, H., Ko, Y. S., Yun, S. P., Park, S. W. & Kim, H. J. P2Y(2)R-mediated transactivation of VEGFR2 through Src phosphorylation is associated with ESM-1 overexpression in radiotherapy-resistant-triple negative breast cancer cells. *Int. J. Oncol.* **62**, https://doi.org/10.3892/ijo.2023.5521 (2023).
41. Antoon, J. W. et al. Inhibition of p38-MAPK alters SRC coactivation and estrogen receptor phosphorylation. *Cancer Biol. Ther.* **13**, 1026–1033 (2012).
42. Stairs, D. B. et al. Deletion of p120-catenin results in a tumor microenvironment with inflammation and cancer that establishes it as a tumor suppressor gene. *Cancer Cell* **19**, 470–483 (2011).
43. Shi, Y. et al. DDX5 promotes esophageal squamous cell carcinoma growth through sustaining VAV3 mRNA stability. *Oncogene* **43**, 3240–3254 (2024).
44. Qin, X. et al. Serotonin/HTR1E signaling blocks chronic stress-promoted progression of ovarian cancer. *Theranostics* **11**, 6950–6965 (2021).
45. Xie, Y. et al. Ornithine decarboxylase inhibition downregulates multiple pathways involved in the formation of precancerous lesions of esophageal squamous cell cancer. *Mol. Carcinog.* **59**, 215–226 (2020).
46. Rapozo, D. C. et al. Recurrent acute thermal lesion induces esophageal hyperproliferative premalignant lesions in mice esophagus. *Exp. Mol. Pathol.* **100**, 325–331 (2016).
47. Chen, X. & Cubillos-Ruiz, J. R. Endoplasmic reticulum stress signals in the tumour and its microenvironment. *Nat. Rev. Cancer* **21**, 71–88 (2021).
48. Ma, Y. & Hendershot, L. M. The role of the unfolded protein response in tumour development: friend or foe? *Nat. Rev. Cancer* **4**, 966–977 (2004).
49. Kaneko, M. et al. ER stress and disease: toward prevention and treatment. *Biol. Pharm. Bull.* **40**, 1337–1343 (2017).
50. Qu, L. et al. Endoplasmic reticulum stress induces p53 cytoplasmic localization and prevents p53-dependent apoptosis by a pathway involving glycogen synthase kinase-3beta. *Genes Dev.* **18**, 261–277 (2004).
51. Aguirre-Ghiso, J. A., Estrada, Y., Liu, D. & Ossowski, L. ERK(MAPK) activity as a determinant of tumor growth and dormancy; regulation by p38(SAPK). *Cancer Res.* **63**, 1684–1695 (2003).
52. Estrada, Y., Dong, J. & Ossowski, L. Positive crosstalk between ERK and p38 in melanoma stimulates migration and in vivo proliferation. *Pigment Cell Melanoma Res.* **22**, 66–76 (2009).
53. Zhao, Y. et al. RPS15 interacted with IGF2BP1 to promote esophageal squamous cell carcinoma development via recognizing m(6)A modification. *Signal Transduct. Target Ther.* **8**, 224 (2023).
54. Chen, J. et al. ACSL4 reprograms fatty acid metabolism in hepatocellular carcinoma via c-Myc/SREBP1 pathway. *Cancer Lett.* **502**, 154–165 (2021).
55. Chen, J. et al. ACSL4 promotes hepatocellular carcinoma progression via c-Myc stability mediated by ERK/FBW7/c-Myc axis. *Oncogenesis* **9**, 42 (2020).
56. Gan, B. ACSL4, PUFA, and ferroptosis: new arsenal in anti-tumor immunity. *Signal Transduct. Target Ther.* **7**, 128 (2022).
57. Liao, P. et al. CD8(+) T cells and fatty acids orchestrate tumor ferroptosis and immunity via ACSL4. *Cancer Cell* **40**, 365–378 e366 (2022).
58. Doll, S. et al. ACSL4 dictates ferroptosis sensitivity by shaping cellular lipid composition. *Nat. Chem. Biol.* **13**, 91–98 (2017).
59. Smith, M. E., Saraceno, G. E., Capani, F. & Castilla, R. Long-chain acyl-CoA synthetase 4 is regulated by phosphorylation. *Biochem. Biophys. Res. Commun.* **430**, 272–277 (2013).
60. Rohrig, F. & Schulze, A. The multifaceted roles of fatty acid synthesis in cancer. *Nat. Rev. Cancer* **16**, 732–749 (2016).
61. Resh, M. D. Covalent lipid modifications of proteins. *Curr. Biol.* **23**, R431–R435 (2013).
62. Jiang, H. et al. Protein lipidation: occurrence, mechanisms, biological functions, and enabling technologies. *Chem. Rev.* **118**, 919–988 (2018).
63. Zhang, Q. et al. ACSL1-induced ferroptosis and platinum resistance in ovarian cancer by increasing FSP1 N-myristylation and stability. *Cell Death Discov.* **9**, 83 (2023).
64. Huang, M. et al. Bioinformatics and network pharmacology identify promotional effects and potential mechanisms of ethanol on esophageal squamous cell carcinoma and experimental validation. *Toxicol. Appl. Pharm.* **474**, 116615 (2023).
65. Yao, J. et al. Single-cell transcriptomic analysis in a mouse model deciphers cell transition states in the multistep development of esophageal cancer. *Nat. Commun.* **11**, 3715 (2020).
66. Gazou, A. et al. Xq22.3-q23 deletion including ACSL4 in a patient with intellectual disability. *Am. J. Med. Genet. A* **161A**, 860–864 (2013).
67. Yang, X. et al. PHLDA2-mediated phosphatidic acid peroxidation triggers a distinct ferroptotic response during tumor suppression. *Cell Metab.* **36**, 762–777 e769 (2024).
68. Loda, A., Collombet, S. & Heard, E. Gene regulation in time and space during X-chromosome inactivation. *Nat. Rev. Mol. Cell Biol.* **23**, 231–249 (2022).
69. Liu, X. et al. Spatial transcriptomics analysis of esophageal squamous precancerous lesions and their progression to esophageal cancer. *Nat. Commun.* **14**, 4779 (2023).
70. Chen, Y. et al. Diosmetin suppresses the progression of ESCC by CDK2/Rb/E2F2/RRM2 pathway and synergies with cisplatin. *Oncogene* **42**, 2278–2293 (2023).
71. Wu, W. et al. TOPK promotes the growth of esophageal cancer in vitro and in vivo by enhancing YB1/eEF1A1 signal pathway. *Cell Death Dis.* **14**, 364 (2023).
72. Dawsey, S. M. et al. Squamous esophageal histology and subsequent risk of squamous cell carcinoma of the esophagus. A prospective follow-up study from Linxian, China. *Cancer* **74**, 1686–1692 (1994).
73. Yang, X., Ma, Y., Li, N., Cai, H. & Bartlett, M. G. Development of a method for the determination of Acyl-CoA compounds by liquid

chromatography mass spectrometry to probe the metabolism of fatty acids. *Anal. Chem.* **89**, 813–821 (2017).
74. Bao, Z. et al. Oxethazaine inhibits esophageal squamous cell carcinoma proliferation and metastasis by targeting aurora kinase A. *Cell Death Dis.* **13**, 189 (2022).
75. Parvin, M. et al. Oroxylum indicum stem bark extract reduces tumor progression by Inhibiting the EGFR-PI3K-AKT pathway in an in vivo 4NQO-induced oral cancer model. *J. Am. Nutr. Assoc.* **42**, 573–587 (2023).

Acknowledgements

This work was supported by the National Natural Science Foundations of China (No.81872335, 82472998, K.L.), National Natural Science Youth Foundation (No. 81902486, Y.J.), National Natural Science Youth Foundation (No.82303891, Y.X.), The Central Plains Science and Technology Innovation Leading Talents (224200510015, K.L.), and the National Natural Science Foundations of China (No. 82473228, Y.J.).

Author contributions

Q.Y.: performed the cell, animal experiments and wrote the manuscript. Y.S.: collected the data from GEO and GEPIA database and assisted in Western blot. J.W.: were engaged in Fatty acyl-CoA analysis by LC-MS/MS and animal experiments. Y.X.: revised the manuscript. X.L.: performed the immunohistochemical studies and assisted in Western blot. J.Z.: discussion. Y.J.: established CDX mice model. Y.Q.: Computer docking model. Y.G.: conducted the data analysis. C.Z.: collected ESCC tissue and adjacent tissue. J.L.: discussion. T.Z.: modify experimental scheme. Z.D.: provided with platform for animal experiments. P.L.: Funding acquisition. Z.G.D.: Funding acquisition. K.L.: designed the project. All authors have read and agreed to the published version of the manuscript.

Competing interests

The authors declare no competing interests.

Additional information

Supplementary information The online version contains supplementary material available at https://doi.org/10.1038/s41467-025-58342-z.

Correspondence and requests for materials should be addressed to Peng Li, Zigang Dong or Kangdong Liu.

Peer review information *Nature Communications* thanks Claudia Andl and the other anonymous reviewer(s) for their contribution to the peer review of this work. A peer review file is available.